Science of the Total Environment 722 (2020) 137824

Contents lists available at ScienceDirect

Science of the Total Environment

journal homepage: www.elsevier.com/locate/scitotenv

Groundwater resources and recharge processes in the Western Andean Front of Central Chile

Matías Taucare [a,b], Linda Daniele [a,b,*], Benoît Viguier [a,b], Angela Vallejos [c], Gloria Arancibia [b,d]

[a] Departamento de Geología, Facultad de Ciencias Físicas y Matemáticas, Universidad de Chile, Santiago, Chile
[b] Centro de Excelencia en Geotermia de los Andes (CEGA), Facultad de Ciencias Físicas y Matemáticas, Universidad de Chile, Santiago, Chile
[c] Recursos Hídricos y Geología Ambiental, Universidad de Almería, Almería, Spain
[d] Departamento de Ingeniería Estructural y Geotécnica, Pontificia Universidad Católica de Chile, Santiago, Chile

HIGHLIGHTS

- Central Depression aquifers receive recharge from mountain-block and -front area.
- Focused recharge originates from rain and snowmelt above 2000 m asl.
- Mountain recharge processes are critical for an effective water management.
- At San Felipe alluvial aquifer, there is anthropogenic recharge by irrigation canals.
- Agriculture impacts the groundwater quality in the Central Depression aquifers.

GRAPHICAL ABSTRACT

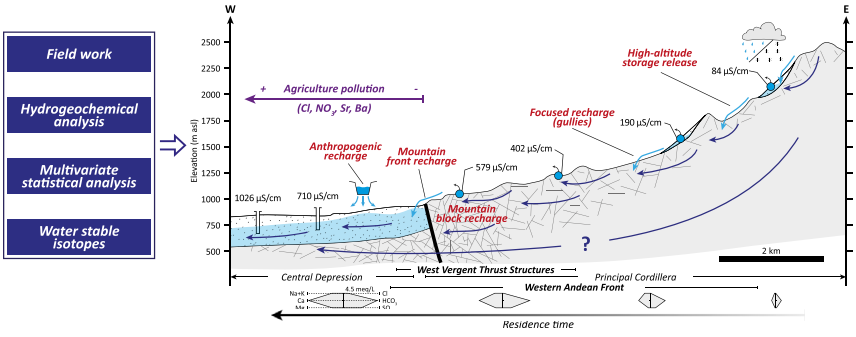

ARTICLE INFO

Article history:
Received 4 December 2019
Received in revised form 4 February 2020
Accepted 7 March 2020
Available online 10 March 2020

Editor: José Virgílio Cruz

Keywords:
Groundwater
Fractured aquifer
Mountain front zone
Hydrogeochemistry
Water stable isotopes
Aconcagua Basin

ABSTRACT

In Central Chile, the increment of withdrawals together with drought conditions has exposed the poor understanding of the regional hydrogeological system. In this study, we addressed the Western Andean Front hydrogeology by hydrogeochemical and water stable isotope analyses of 23 springs, 10 boreholes, 5 rain-collectors and 5 leaching-rocks samples at Aconcagua Basin. From the upstream to the downstream parts of the Western Andean Front, most groundwater is HCO_3-Ca and results from the dissolution of anorthite, labradorite and other silicate minerals. The Hierarchical Cluster Analysis groups the samples according to its position along the Western Andean Front and supports a clear correlation between the increasing groundwater mineralization (31–1188 µS/cm) and residence time. Through Factorial Analysis, we point that Cl, NO_3, Sr and Ba concentrations are related to agriculture practices in the Central Depression. After defining the regional meteoric water line at 33°S in Chile, water isotopes demonstrate the role of rain and snowmelt above ~2000 m asl in the recharge of groundwater. Finally, we propose an original conceptual model applicable to the entire Central Chile. During dry periods, water releases from high-elevation areas infiltrate in mid-mountain gullies feeding groundwater circulation in the fractured rocks of Western Andean Front. To the downstream, mountain-block and -front processes recharge the alluvial aquifers. Irrigation canals, conducting water from Principal Cordillera, play a significant role in the recharge of Central Depression aquifers. While groundwater in the Western Andean Front has a high-quality according to different water uses, intensive agriculture practices in the Central Depression cause an increment of hazardous elements for human-health in groundwater.

* Corresponding author at: Departamento de Geología, Facultad de Ciencias Físicas y Matemáticas, Universidad de Chile, Santiago, Chile.
E-mail address: ldaniele@ing.uchile.cl (L. Daniele).

https://doi.org/10.1016/j.scitotenv.2020.137824
0048-9697/

1. Introduction

In arid environments, the extraction of groundwater from aquifers plays a strategic role in the development of social-economic activities (*e.g.* drinking water, agriculture, industry, tourism, *etc.*). But the increasing anthropogenic and climatic pressures critically impact the availability of usual groundwater resources contained in shallow alluvial aquifers. The implementation of sustainable aquifer management policies fundamentally depends on a good understanding of the aquifer functioning (Simmers, 1997). Indeed, the hydrogeological inaccuracies or inclination to oversimplify the hydrogeological conceptual models may lead to unsuitable management policies, strengthening the risk to overexploit the groundwater resources (Huggenberger and Aigner, 1999; Scanlon et al., 2006; Kresic and Mikszewski, 2012; Viguier et al., 2019). In such context, it is a matter of urgency to assess (or update) the regional hydrogeological conceptual models.

In Central Chile (32°S-36°S, Fig. 1a), the exploration of groundwater resources was focused on Quaternary alluvial deposits filling valley

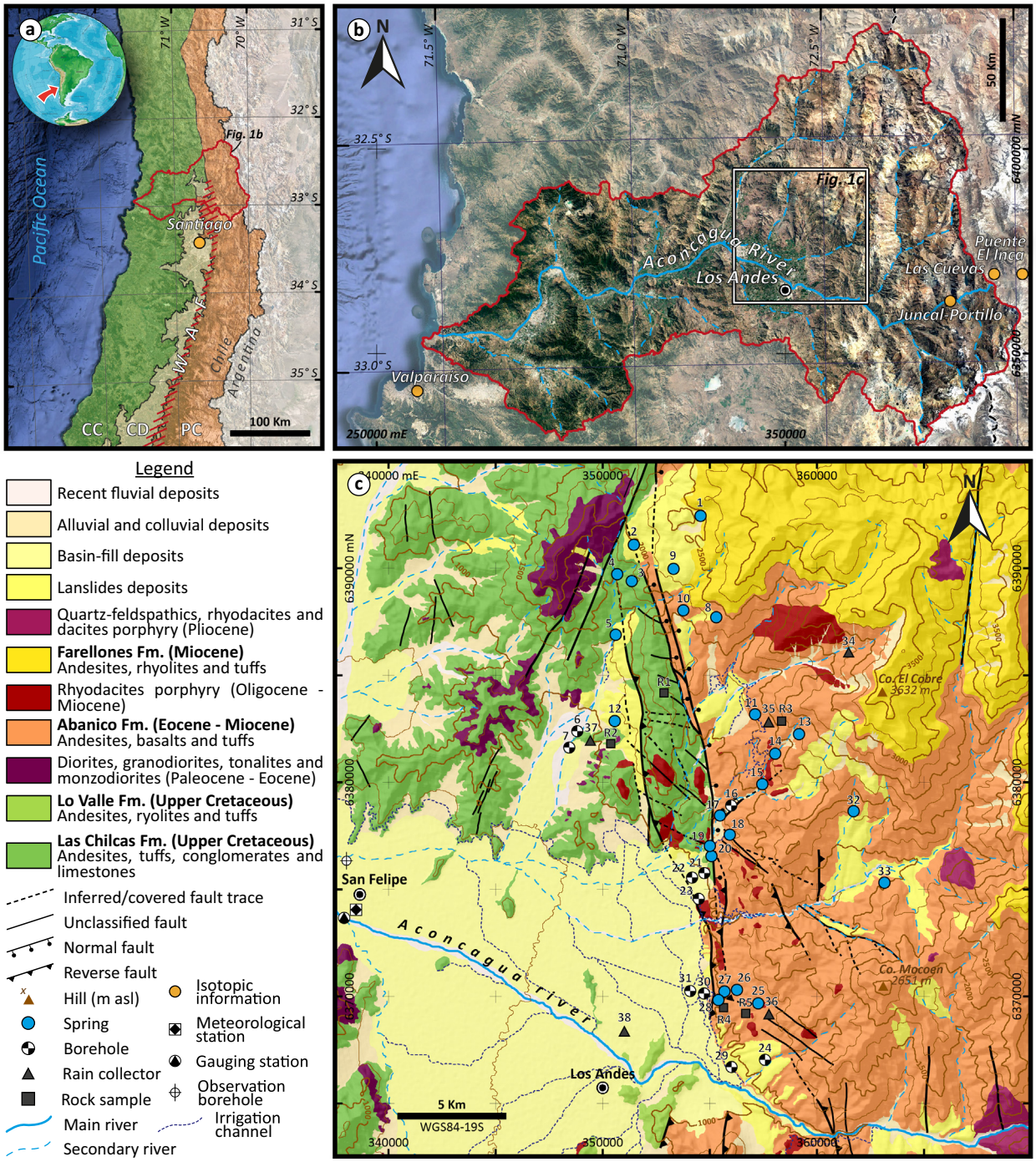

Fig. 1. Location of the study area. a) Localization of Aconcagua Basin (red area) in Central Chile and the main Andean morphotectonic domains: Coastal Cordillera (CC), Central Depression (CD) and the Principal Cordillera (PC). The Western Andean Front (WAF) is shown by red diagonal lines. b) Location of the study area in Aconcagua Basin. c) Geological map of the study area (based on Rivano et al., 1993; Fuentes, 2004; Jara and Charrier, 2014; Boyce et al., 2020) and location of sampled points.

bottoms and basin floors in the Central Depression (DPRH, 2015). As a result, numerous inaccuracies and unverified assumptions exist regarding both the groundwater circulation and the recharge processes along the western flank of the Andes (*i.e.* Western Andean Front), at the interface between the Principal Cordillera (3000–6000 m asl) and the Central Depression (200–800 m asl). However, groundwater recharge from mountain front zones typically ranges from 5 up to 50% (Markovich et al., 2019) suggesting that the Western Andean Front may contribute to recharge alluvial aquifers in the Central Depression. Indeed, the precipitation rate in the Principal Cordillera is around two times higher than in the Central Depression (provided by *Dirección General de Aguas* for the period between 1980 and 2018; DGA, 2019), and several perennial springs along the Western Andean Front evidence groundwater circulation through fractured rocks in Principal Cordillera (Benavente et al., 2016). Unlike different authors have addressed the role of the western Andean Piedmont in the recharge of Central Depression aquifers in the Atacama Desert at Northern Chile (*e.g.* Magaritz et al., 1990; Houston, 2002; Nester et al., 2007; Viguier et al., 2018; Gamboa et al., 2019; Marazuela et al., 2019), the Western Andean Front in Central Chile is arbitrary fixed as a no-flux boundary condition in Central Depression aquifer flow modelling (DGA, 2015, 2016).

In addition to the misunderstanding of fluxes in the Western Andean Front, Central Chile has experienced an interrupted sequence of dry years since 2010, known as "Megadrought" (Garreaud et al., 2019), with rainfall deficits between 20% and 40%. The combined effects of continuous dry years and increasing withdrawals (essentially for intensive agriculture activities) have led to overexploit shallow alluvial aquifers leading to dry rivers fed by groundwater. Nowadays, social tensions are emerging between water resource users, especially since water management is based on the principle of water private rights that limit the equity of water resource repartition (Valdés-Pineda et al., 2014; Costumero et al., 2016; Rivera et al., 2016).

Considering the alarming state of water resources in Central Chile, regional hydrogeological conceptual models must be improved to better point the management policies. Consequently, we assess the groundwater circulation and related recharge processes taking place in the Western Andean Front as well as its role in the recharge of Central Depression aquifers (*i.e.* mountain-front and mountain-block processes). The study was carried out in an emblematic area gathering all water resources concerns of Central Chile: the Aconcagua Basin (Fig. 1).

2. The study area: the Aconcagua Basin

2.1. Geological setting

The Andes results from several compressional phases alternated by extensional ones since the middle Cretaceous (Mpodozis and Ramos, 1989; Arancibia, 2004; Charrier et al., 2007). As a consequence, the Andean region of Central Chile (32°-36°S) is segmented into three major NS-oriented morphotectonic domains (Jordan et al., 1983), from west to east (Fig. 1a): i) the Coastal Cordillera (up to 2000 m asl), ii) the Central Depression (~570 m asl) and iii) the Principal Cordillera (up to 5000–6000 m asl).

The western flank of the Principal Cordillera (referred hereafter as "Western Andean Front") is a first-order morphological feature associated with a topographical difference of >2000 m relative to the Central Depression (Rauld, 2011). Along Central Chile, the Western Andean Front is shaped by west vergent thrust structures (Armijo et al., 2010; Farías et al., 2010; Vargas et al., 2014). These latter played as normal faults between the late Eocene and Oligocene, and then were reactivated as reverse faults during the late Miocene and early Pliocene (Godoy et al., 1999; Jordan et al., 2001; Charrier et al., 2002). An emblematic example is the Pocuro Fault Zone (PFZ) at Aconcagua Basin, which records those tectonics events along a NS-oriented brittle deformation zone spanning over 150 km long and 4 km wide.

In the study area (Fig. 1c), a thick volcano-sedimentary sequence intruded by coeval plutonic rocks is exposed, which results from the eastward migration of the magmatic arc and sedimentary processes (Parada et al., 1988; Kay et al., 2005):

- Las Chilcas Formation (middle to late Cretaceous) located in the Coastal Cordillera comprises ~6000 m of basalts, andesites and pyroclastic rocks intercalated by sedimentary layers cemented by calcite and iron oxides (Thomas, 1958; Wall et al., 1999; Boyce et al., 2020).
- Lo Valle Formation (late Cretaceous) outcrops as *inselberg* into the Central Depression and it is constituted by 700–1800 m of dacitic tuff with intercalations of porphyritic andesites (Thomas, 1958; Gana and Wall, 1997; Boyce et al., 2020).
- Abanico Formation (late Eocene to early Miocene) located in the Principal Cordillera is made up by ~3000 m of andesites, basalts and pyroclastic rocks intercalated with conglomerates, sandstones and mudrocks (Fuentes et al., 2002; Nyström et al., 2003; Muñoz et al., 2006; Jara and Charrier, 2014; Piquer et al., 2017).
- Farellones Formation (early to middle Miocene) outcrops in the highest part of the Principal Range and it is a 1000–2500 m thick sequence of dacitic-rhyolitic tuff, andesites and rhyolites (Rivano et al., 1990; Fuentes et al., 2002; Nyström et al., 2003; Jara and Charrier, 2014; Piquer et al., 2017).

Subsequent erosional processes (post Pliocene) in the Principal Cordillera, originated detrital materials which were transported along EW-oriented fluvio-glacial valleys, such as the Aconcagua River (Fig. 1b). Then, the transport of detrital materials allows the filling of the Central Depression basin floor, with an average thickness of ~300 m (Yáñez et al., 2015).

2.2. Hydro(geo)logical setting

2.2.1. Hydroclimatic variability

Central Chile is characterized by a semi-arid climate where moisture fluxes originate from the Pacific Ocean and cold fronts associated with low pressure systems (Barrett et al., 2009). The Principal Cordillera acts as an orographic barrier isolating the western flank of the Chilean Andes from the Atlantic influence (Barrett et al., 2009). During the historic time-period (1980–2010), annual precipitation averaged 520 mm/year in the Coastal Cordillera, 280 mm/year in the Central Depression and 620 mm/year in the Principal Cordillera according to the database of *Dirección General de Aguas* (DGA) (DGA, 2019). Typically, most of precipitation (~65%) occurs during the austral winter. The interannual variability is typically related to El Niño Southern Oscillation (ENSO) (Montecinos and Aceituno, 2003) showing wet and dry years during El Niño and la Niña phases, respectively (Fig. 2a). In the interface between the Central Depression and the Principal Cordillera, the Western Andean Front is a hydroclimate transition area where the 0 °C isotherm line oscillates around 2000 m a.s.l. In the mountain front zone at 1100 m asl , air temperature averages 15 °C and ranges from −5 °C during the austral winter to 38 °C during the austral summer (DGA, 2019).

On mountain flanks, several temporary streams occur after anomalous rainy events (Garreaud, 2013; Viale and Garreaud, 2014) unlike major exorheic perennial streams originating from the Principal Cordillera (*e.g.* Aconcagua River; Fig. 1b). Perennial streams are fed by precipitation during wet time periods whereas groundwater and snowmelt on highs support the river base-flow during dry time periods (Waylen and Caviedes, 1990; Cortés et al., 2011; Ohlanders et al., 2013). However, since 2010 the "Megadrought", characterized by an interrupted sequence of dry years uncorrelated from the ENSO variations (Fig. 2a and b), has led to an alarming rainfall deficit from 25 to 45% in Central Chile related to the historic period (1980–2010) (Boisier et al., 2016; Garreaud et al., 2017). Although snowmelt on highs support the river discharges (Ohlanders et al., 2013; Janke et al., 2017; Schaffer et al.,

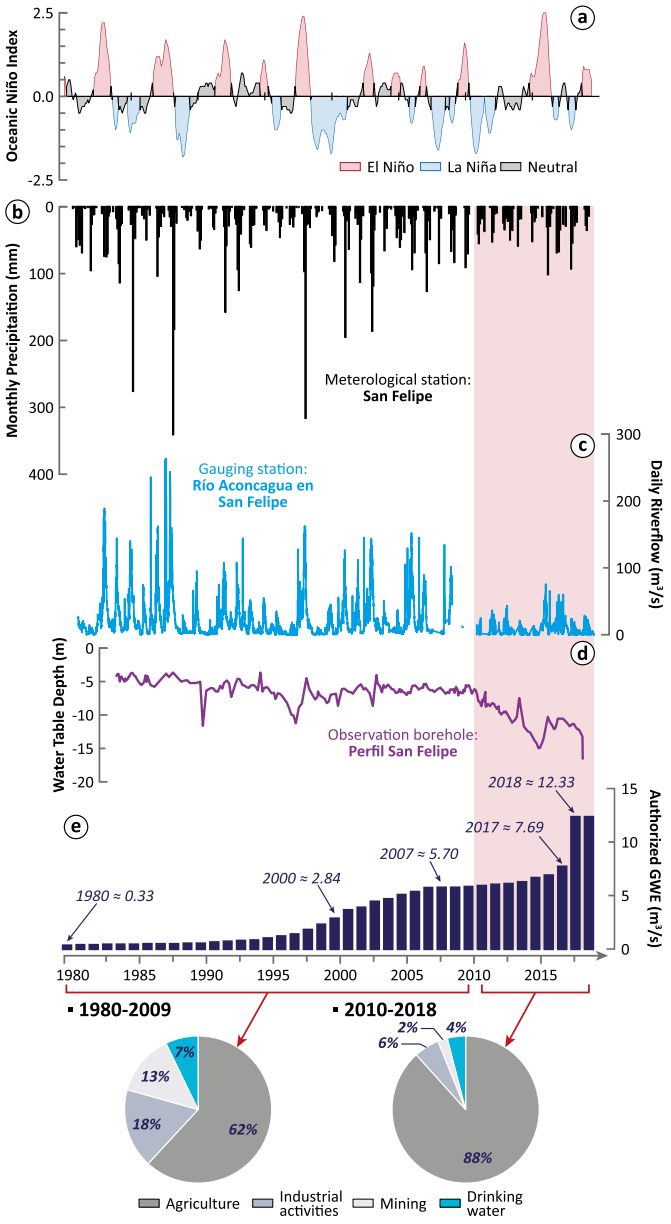

Fig. 2. Hydro(geo)logical context in the Aconcagua Basin. Hydroclimatic time series since 1980 to the present: a) Oceanic Niño Index (NOAA/National Weather Service, 2019); b) monthly precipitation at "*San Felipe*" meteorological station; c) daily riverflow at "*Río Aconcagua en San Felipe*" gauging station; d) water table depth (meters below ground surface) at the "*Perfil San Felipe*" observation borehole; e) authorized groundwater extraction in the San Felipe aquifer and respective uses during the historic time-period (1980–2009) and the megadrought (2010–2018). In pink is highlighted the "Megadrought" of Central Chile. b), c), d) and e) available data at DGA web site (DGA, 2019). All point location visible in Fig. 1.

2019), surface water resources have rapidly declined up to 90% (Garreaud et al., 2017) leading the drought of many rivers (Fig. 2c).

2.2.2. Groundwater resources

Along the Western Andean Front at least 23 perennial springs outflow from fractured rocks at different elevations (Fig. 1c). Major springs were described first by Darwin (1839) and have been used for thermal-bath activities and mineral water bottling over decades, especially due to the stability in physico-chemical parameters and geochemical composition (Darapsky, 1890; Hauser, 1997; Bustamante et al., 2012; Benavente et al., 2016). Despite the previous studies, the groundwater circulation and related recharge processes taking place in the Western Andean Front remain so far undescribed.

To the West, in the Central Depression, the San Felipe aquifer is contained into the Quaternary alluvial sediments (200–360 m thick) filling the Aconcagua Basin (DGA, 2015, 2016). According to DGA (2016), the San Felipe aquifer is limited by the PFZ and the volcano-sedimentary sequences that are considered as no-flux boundary conditions. Groundwater recharge is exclusively related to diffuse recharge from precipitation as well as to focused recharge from Aconcagua River. Historically, surface-water coming from Principal Cordillera and distributed by canals (Fig. 1b) has permitted the development of small farming activities in the Central Depression. But since the late 1980s, the implementation of intensive agriculture practices, especially avocado, olives and grapevine cultivation has led to an increment of the water demand (Novoa et al., 2019). As a consequence, the authorized groundwater extraction from the San Felipe alluvial aquifer has significantly increased leading to a progressive water table decline (Fig. 2d and e). In fact, withdrawals from the San Felipe aquifer have increased further during the "Megadrought" (Fig. 2e). It results in an alarming and sharp water table drop (~10 m; Fig. 2d). Nowadays, groundwater resources in the Central Depression are overexploited. Current state of groundwater resources makes necessary to reliably assess the groundwater circulation in the Western Andean Front and its role in the recharge of alluvial aquifers.

3. Methodology

3.1. Sampling and analysis

Between February 2017 and September 2018, we collected a total of 33 groundwater samples for geochemical and isotopic analyses: 23 springs and 10 boreholes (Table 1 and Fig. 1c). Additionally, 5 rain collectors were installed between 830 and 2715 m asl. A paraffin oil layer was inserted into each collector to avoid any evaporation and isotope fractioning process (IAEA/GNIP, 2014). Electrical conductivity, temperature and pH were measured *in situ*. Water samples were filtered using 0.45 μm Millipore filters. Unacidified samples were collected for anion analysis, and acidified samples (Suprapur® Nitric acid) for cations and trace elements analysis. Unfiltered samples were collected for stable isotope analysis. All samples were stored in pre-cleaned polyethylene bottles at 4 °C.

Major, minor and trace elements were analyzed at Andean Geothermal Center of Excellence (CEGA) of the Geology Department (University of Chile). Cl, SO_4 and NO_3 contents were determined by Ion Chromatography (IC, 861 Compact IC Metrohm) with a detection limit of 0.030, 0.070 and 0.100 ppm, respectively. SiO_2, Na, K, Ca and Mg were measured by Atomic Absorption Spectrophotometry (F-AAS, Perkin-Elmer PinAAcle 900F) with detection limits of 0.1, 0.094, 0.044, 0.014 and 0.010 ppm, respectively. Li, B, As, Sr and Ba contents were determined by Inductively Coupled Plasma Mass Spectrometry (ICP-MS, Thermo iCAP Q) with detection limits of 0.020, 0.070, 0.020, 0.001 and 0.010 ppb, respectively. Alkalinity (as HCO_3) was determined by titration at the sampling time to prevent precipitation of carbonates, by using HCl (0.1 N) as limiting reagent. $\delta^{18}O$ and δD (water stable isotopes) were analyzed by Finnigan Delta Plus XL mass spectrometer at *Estación Experimental de Zaidín* (CSIC, Spain) with an analytical uncertainty of ±0.1‰ and ± 1.1‰ VSMOW, respectively.

3.2. Ionic extraction by leaching test

One way to get information about the source of dissolved solids in groundwater is comparing them with the composition of rocks where groundwater circulation occurs (Kaasalainen and Stefánsson, 2012). Five fresh rock samples were collected from representative outcrops of Las Chilcas and Abanico Formation in the Western Andean Front

Table 1
Chemical and isotopic analysis of spring, borehole and meteoric water samples.

Sample Id	Source	Altitude (m asl)	T°C	pH	EC (μS/cm)	Major elements (ppm)									Trace elements (ppb)					Ionic ratios (meq/L)				Stable isotopes	
						SiO_2	Cl	SO_4	HCO_3	NO_3	Na	K	Ca	Mg	Li	B	As	Sr	Ba	rNa/rCa	rMg/rCa	rLi/rCl	rB/rCl	δD (VSMOW)	$\delta^{18}O$ (VSMOW)
1	Spring	2465	27.7	8.17	31	11.0	0.08	0.9	15.1	0.21	0.42	*bdl*	3.08	0.40	*bdl*	3.30	0.40	17.50	2.19	0.364	0.346	0.0017	0.183	−69.52	−6.31
2	Spring	1933	13.5	7.38	84	20.9	0.44	2.9	44.1	2.45	4.66	0.13	10.45	0.83	*bdl*	8.38	0.86	18.02	0.62	0.173	0.276	0.0011	0.024	−86.24	−11.31
3	Spring	1562	20.4	8.40	190	15.8	1.07	18.7	89.8	0.34	31.88	0.51	7.09	0.23	1.36	20.11	1.40	5.54	0.62	0.311	0.500	0.0053	0.184	−88.17	−11.02
4	Spring	1515	14.9	7.82	278	22.2	0.92	4.2	174.6	0.43	11.88	*bdl*	42.68	4.30	0.83	49.98	2.72	77.13	4.19	0.283	0.311	0.0028	0.207	−86.262	−10.840
5	Spring	1246	17.2	8.47	277	23.1	1.63	24.3	131.4	5.64	17.28	0.37	36.78	4.11	2.89	78.69	8.35	176.64	5.49	0.295	0.327	0.0033	0.199	−92.56	−11.18
6	Borehole	938	22.4	7.16	519	32.6	7.91	78.5	225.8	12.87	28.08	1.47	67.22	14.11	2.56	147.19	3.71	309.07	23.76	0.453	0.411	0.0039	0.141	−78.94	−9.41
7	Borehole	895	23.2	7.48	703	33.9	23.34	41.5	338.6	34.97	20.92	1.67	105.36	17.63	5.08	56.64	0.97	439.92	48.00	0.410	0.360	0.0008	0.059	−85.54	−10.76
8	Spring	2380	21.0	7.09	168	18.0	0.50	2.4	73.2	0.34	5.00	*bdl*	16.38	1.57	*bdl*	6.28	0.62	54.08	1.39	0.399	0.189	0.0050	0.034	−83.67	−11.43
9	Spring	2301	12.5	7.95	96	26.0	0.96	2.5	37.6	2.29	6.88	0.49	9.16	1.05	*bdl*	6.54	1.17	24.87	1.73	0.287	0.310	0.0024	0.018	−92.34	−12.77
10	Spring	2085	13.3	7.90	144	18.0	0.24	11.5	85.4	2.70	9.10	*bdl*	20.16	1.39	0.25	13.12	1.51	49.79	1.86	0.272	0.278	0.0026	0.026	−92.33	−13.15
11	Spring	1784	21.9	7.13	186	20.1	2.75	39.6	70.2	0.11	17.10	0.40	18.32	1.86	2.33	186.69	3.29	118.91	0.84	0.410	0.184	0.0091	0.475	−84.60	−10.07
12	Spring	1128	21.5	7.43	647	29.5	5.92	185.6	164.7	9.90	26.68	2.35	74.88	22.70	6.18	110.45	12.27	287.32	15.80	0.145	0.210	0.0041	1.506	−72.33	−7.49
13	Spring	2179	23.4	6.97	204	20.1	1.68	44.8	82.4	1.01	6.13	1.38	29.80	2.91	1.43	176.80	12.51	58.28	0.69	0.246	0.257	0.0022	0.405	−81.92	−11.59
14	Spring	1783	18.9	7.41	330	21.7	1.21	52.7	161.7	2.43	9.11	0.54	54.76	6.98	0.98	185.46	1.59	104.05	1.92	0.239	0.254	0.0029	0.339	−85.76	−11.36
15	Spring	1490	21.0	8.52	272	25.0	2.10	34.9	140.3	2.89	17.55	1.04	38.30	4.12	1.27	130.16	7.80	81.64	1.24	0.387	0.216	0.0041	0.217	–	–
16	Borehole	1283	22.2	7.36	412	24.9	2.89	73.4	180.0	5.67	17.19	0.63	60.86	9.50	1.26	118.95	9.28	142.56	6.33	0.251	0.292	0.0034	0.247	−78.30	−9.79
17	Spring	1239	22.8	7.14	461	26.2	3.41	74.7	225.8	5.42	19.55	0.38	71.22	10.95	1.91	117.23	1.69	67.90	4.31	0.279	0.349	0.0052	0.240	−74.10	−7.61
18	Spring	1157	25.7	8.19	484	27.0	4.03	56.0	241.0	5.17	29.10	0.04	65.59	8.60	3.27	88.69	2.99	253.80	5.33	0.435	0.273	0.0006	0.020	–	–
19	Spring	1088	21.0	7.10	575	28.1	4.89	97.7	265.4	9.47	24.80	0.27	86.22	15.29	3.25	122.95	2.84	125.17	0.58	0.443	0.316	0.0069	0.086	−75.50	−10.05
20	Spring	1077	22.3	7.22	557	29.9	4.55	73.6	286.8	11.78	24.96	0.69	78.14	16.55	4.65	111.04	12.74	332.71	1.92	0.384	0.343	0.0048	0.071	−72.63	−8.97
21	Borehole	980	21.0	7.54	686	32.0	5.86	93.6	305.1	9.48	28.80	0.65	88.80	16.77	3.22	123.07	5.06	381.86	61.06	0.430	0.350	0.0072	0.108	−83.48	−11.40
22	Borehole	973	23.2	7.55	644	37.0	6.01	77.5	244.1	16.43	29.10	0.63	85.88	17.01	3.85	121.06	5.73	399.18	67.20	3.921	0.053	0.0065	0.185	−83.42	−11.31
23	Borehole	939	21.4	7.77	581	34.0	7.18	56.4	244.1	37.50	32.70	0.53	62.96	15.69	5.48	102.67	6.78	379.10	8.63	0.243	0.166	0.0046	0.536	−85.33	−12.01
24	Borehole	1146	20.8	7.43	570	31.0	12.21	22.3	192.3	11.90	24.15	0.51	48.43	8.01	1.46	25.15	2.69	290.66	2.51	0.394	0.113	0.0053	0.545	–	–
25	Spring	1088	23.7	7.45	275	31.6	2.48	10.1	170.8	9.02	17.54	0.64	34.50	6.62	3.34	21.71	3.24	136.20	2.21	0.814	0.167	0.0043	0.669	−73.15	−8.73
26	Spring	993	19.8	7.37	402	26.8	8.67	33.4	201.4	7.27	21.12	3.91	47.92	9.98	8.23	62.69	9.13	341.36	3.11	0.179	0.161	0.0043	1.037	−75.68	−9.62
27	Spring	981	20.6	7.66	390	26.0	6.19	36.3	195.3	6.92	23.20	0.73	47.00	9.97	8.73	68.05	8.87	345.97	3.27	0.400	0.177	0.0031	0.610	−73.59	−8.17
28	Spring	975	24.1	7.95	579	24.8	14.26	55.4	302.0	4.39	33.82	6.47	71.88	15.69	2.30	85.81	5.06	421.58	14.84	0.292	0.155	0.0029	0.493	−76.60	−7.89
29	Borehole	919	18.9	6.99	1188	25.8	60.17	166.4	197.1	10.29	48.20	0.90	105.35	12.10	58.66	209.41	22.05	927.64	11.48	0.119	0.214	0.0012	0.396	–	–
30	Borehole	918	18.6	7.59	710	27.0	30.01	140.9	256.3	9.66	30.90	0.93	93.95	17.66	14.30	53.77	3.98	715.44	14.52	0.389	0.131	0.0002	0.189	−107.92	−15.38
31	Borehole	889	–	7.68	1026	25.8	28.04	141.6	256.3	9.35	32.00	1.42	102.65	17.30	14.12	73.70	3.00	753.15	24.57	0.266	0.158	0.0002	0.123	–	–
32	Spring	1701	11.5	7.96	83	17.6	0.50	10.2	42.7	0.83	1.03	0.24	12.13	1.32	*bdl*	16.07	1.40	19.97	1.04	0.655	0.190	0.0001	0.067	−87.18	−11.71
33	Spring	1456	18.0	7.72	341	22.9	1.697	62.6	134.2	*bdl*	15.46	*bdl*	46.20	4.34	0.97	84.95	2.84	125.17	0.58	0.074	0.179	0.0002	0.319	−83.35	−11.59
34	Meteoric	2715	15.7	5.87	14	*bdl*	1.01	0.7	1.0	1.59	0.30	0.73	1.79	0.00	*bdl*	*bdl*	0.21	3.66	4.05	0.146	0.001	0.0001	0.001	–	–
35	Meteoric	1965	15.6	6.17	45	0.3	0.53	2.1	16.9	*bdl*	0.45	1.16	6.89	0.22	0.54	24.30	1.73	11.36	2.32	0.057	0.053	0.0052	0.452	−101.80	−12.99
36	Meteoric	1132	14.2	5.70	28	*bdl*	1.19	1.9	7.6	*bdl*	0.48	2.92	2.24	0.29	*bdl*	4.15	1.30	12.13	4.08	0.186	0.215	0.0001	0.034	−70.34	−10.29
37	Meteoric	970	14.5	6.70	50	*bdl*	1.95	2.5	15.7	*bdl*	1.22	8.74	3.01	0.66	*bdl*	13.08	0.94	8.24	4.84	0.353	0.361	0.0001	0.066	−66.43	−9.53
38	Meteoric	830	15.0	6.68	56	1.5	0.56	3.4	22.0	*bdl*	0.19	0.57	11.77	0.22	*bdl*	6.75	1.03	19.27	10.14	0.014	0.031	0.0002	0.119	–	–
			Detection limits:			0.1	0.03	0.07	0.0	0.10	0.09	0.04	0.014	0.001	0.02	0.07	0.02	0.001	0.01						

Table 2
Chemical composition of the leaching rock samples.

Id	Lithology	Geological formation	Major elements (ppm)							Trace elements (ppb)					Ionic ratios (meq/L)			
			Cl	SO_4	NO_3	Na	K	Ca	Mg	Li	B	As	Sr	Ba	rNa/rCa	rMg/rCa	rLi/rCl	rB/rCl
R1	Lithic-rich andesitic lapilli-tuff	Las Chilcas	43.88	12.68	8.36	4087	7486	90807	11638	19	46	68	402	220	0.039	0.211	0.0022	0.010
R2	Arkose	Las Chilcas	39.79	226.08	5.30	34793	14393	39053	14911	19	19	74	883	1854	0.777	0.630	0.0025	0.005
R3	Lithic-rich andesitic lapilli-tuff	Abanico	42.61	9.36	8.94	22171	11399	33147	8450	23	59	37	648	448	0.583	0.420	0.0028	0.014
R4	Hydorthermally altered crystal-rich andesitic tuff	Abanico	39.95	17.19	8.21	40924	14122	29661	16754	24	9	8	555	474	1.203	0.931	0.0030	0.002
R5	Lithic-rich andesitic agglomerate	Abanico	24.59	83.09	4.53	28262	10500	32748	9519	16	19	18	431	282	0.753	0.479	0.0034	0.008

(Fig. 1c and Table 2). All rocks were pulverized using a tungsten mortar and sieved to obtain a fine particle size (<39 μm). Cl, SO_4 and NO_3 were extracted using 2 g of rock sample in 100 ml of Milli-Q Water by ultrasound-assisted leaching with a 50 Hz frequency (*e.g.* Güngör and Elik, 2007). At end of leaching, the separation of the final solution from the solid residue was accomplished by centrifugation at 3000 rpm during 10 min. Samples obtained were collected and filtered through a 0.45 μm Millipore filters and analyzed. Na, K, Ca, Mg, Li, B, As, Sr and Ba were extracted by acid digestion bomb method (Matusiewicz, 2003; Wang et al., 2019) using 0.1 g of sample that was dissolved in a mixture of 1.2 ml of HNO_3 and 1.0 ml of HF at 135 °C during 24 h on a hot plate. After cooling at 25 °C, 2 ml of the solution were dissolved with a mixture of 1 ml HCl and 3 ml HNO_3, and heated again at 135 °C during 24 h. In both cases, the resulting solutions have been analyzed at the CEGA laboratories. Note that HCO_3 concentrations have not been obtained from the leaching test because the anion extraction was carried out using Mili-Q Water in laboratory without the presence of CO_2.

3.3. Multivariate statistical analysis

We used the Multivariate statistical analyses to classify the water samples by hydrogeochemical similarities and to study the correlations between the geochemical variables. In this study, two multivariate methods were applied using the IBM SPSS Statistics Software V26: the hierarchical cluster analysis (HCA) and the factorial analysis (FA). Both methods are useful for hydrogeological studies (Moya et al., 2015; Moeck et al., 2016; Negri et al., 2018). The preprocessing stage consists to discard (Cloutier et al., 2008): i) additive characteristics (such as electrical conductivity that is directly related to ion contents), ii) variables with an elevated number of samples below the detection limit, iii) variables that were not analyzed in all samples (*e.g.* $\delta^{18}O$ and δD), and iv) the variables with insignificant regional variations (*e.g.* temperature, pH and K). Concentration values that are lower than the detection limits were replaced by half of the detection limit value. Then, to minimize or eliminate the presence of outliers and the high biased, typical for compositional data (Filzmoser et al., 2009), log-transformation was applied on raw data prior to multivariate analysis. Finally, all statistical analyses were performed using the Cl, SO_4, HCO_3, NO_3, Na, Ca, Mg, SiO_2, Li, B, As, Sr and Ba as variables.

HCA was performed to determine the relationships between the samples using the Euclidian distance as linkage rule (Moeck et al., 2016). The use of HCA allows highlighting the most distinctive geochemical clusters (Güler et al., 2002). The similarity between clusters is expressed by the Euclidean linkage distance in a dendrogram. FA allows identifying the relationships between the geochemical variables by a small number of uncorrelated factors (Giménez-Forcada et al., 2017; Negri et al., 2018). The KMO test was used to determine the factors that explain the variance of the geochemical variables (Kayser, 1960). In this study the KMO value of 0.84 (KMO > 0.7) ensures the quality of the FA. To an accurate analysis, these factors must have eigenvalues higher than one. The factors were rotated using varimax method to maximize the variance of the squared loading for each factor. Finally, the variable weights in each factor is relevant if it is >0.50 (Table 3).

3.4. Local meteoric water line construction

The analyzed stable water isotopes were compared to those contained in precipitation in order to characterize the hydrological processes in the study area (Fig. 1b) and identify the areas contributing to the groundwater recharge. Sánchez-Murillo et al. (2018) have recently proposed a Chilean meteoric water line ($\delta D = 7.47\delta^{18}O + 3.42$) considering hydrological stations along Chile as a whole. But this latter is not completely representative for the study area. Indeed, due to the origin and temporal variations of the moisture fluxes, the meteoric $\delta^{18}O$ and δD are mainly enriched to the North and depleted to the South (Aravena et al., 1999; Garreaud, 2009; Garreaud et al., 2013). Moreover, in Central Chile, the orographic-continental effect is the dominant factor that controls the meteoric $\delta^{18}O$ and δD variations across EW-transect (Jorquera et al., 2015).

Hence, for an accurate characterization of the hydrological processes in the study area, it was necessary to define a reliable local meteoric water line at 33°S in Chile, hereafter "*33°S Chile MWL*". We used available data of $\delta^{18}O$ and δD annual weight means in precipitation (Hoke et al., 2013; IAEA/WMO, 2019) from the Coastal Cordillera, the Central Depression and the Principal Cordillera (Fig. 1b and Table 4). Available $\delta^{18}O$ and δD averages in snowpack, collected between 2200-–2600 and 2600–3000 m asl in the Principal Cordillera by Ohlanders et al. (2013) were also used to attempt characterizing the role of snow in the recharge of groundwater. Analyzed $\delta^{18}O$ and δD in collected rainwater (no. 35, 36, 37) during this study were also compared to those from regional literature.

Table 3
Factorial analysis with Varimax rotation. Both factors describe 82.62% of the data set variance. Weight values > 0.5 are marked in bold.

Variables	Components	
	Factor 1	Factor 2
Cl	**0.49**	**0.76**
SO_4	**0.83**	0.42
HCO_3	**0.92**	0.28
NO_3	**0.53**	**0.62**
Na	**0.87**	0.31
Ca	**0.85**	0.45
Mg	**0.87**	0.35
SiO_2	**0.87**	0.02
Li	**0.76**	0.49
B	**0.89**	0.15
As	**0.76**	0.27
Sr	**0.75**	**0.59**
Ba	−0.02	**0.92**
Variance (%)	58.25	24.37
Cumulative variance (%)	58.25	82.62

Table 4
Dataset of annual weight-mean in precipitation and average in snowpack.

Precipitation							
Station	Reference	Spanning Period	Nbre of w-mean	Lat. (°South)	Long. (°West)	Altitude (m asl)	Morphotectonic domain
Valparaíso	IAEA/WMO (2019)	1988–1991	4	33.06	71.60	74	Coastal Cordillera
Santiago	IAEA/WMO (2019)	1972–1975 1989–1999 2011–2015	20	33.45	70.70	520	Central Depression
Puente el Inca	Hoke et al. (2013)	2008–2009	2	32.82	69.92	2750	Principal Cordillera
Las Cuevas	Hoke et al. (2013)	2008–2009	2	32.81	70.05	3200	Principal Cordillera
Snow							
Station	Reference	Spanning period	Nbre of average	Lat. (°South)	Long. (°South)	Altitude (m asl)	Morphotectonic domain
Juncal-Portillo	Ohlanders et al. (2013)	August 2011	1 1	32.86	70.14	2200–2600 2600–3000	Principal Cordillera

4. Results and discussion

4.1. Hydrogeochemical patterns in the Western Andean front

In the study area, the electrical conductivity (EC) in groundwater ranges from 31 to 1188 μS/cm and increases as elevation decreases (Table 1 and Fig. 3). High-elevation springs (>2000 m asl) have EC values between 31 and 168 μS/cm. Springs and boreholes at lower elevation into the Western Andean Front (<2000 m asl) have EC values between 143 and 647 μS/cm. Finally, in the alluvial San Felipe aquifer, the boreholes display EC values between 519 and 1188 μS/cm. Groundwater temperature in spring mainly agrees with the local mean annual air temperature. But daily fluctuations can be observed in the outflowing water, especially in high-elevation areas, such as visible in the spring no. 1 (located at 2465 m asl) where the measured temperature is 27 °C. Some springs in the PFZ (*e.g.* no. 12, 19, 28) have a permanent low-thermal component (21 to 24 °C) with respect to the local mean annual air temperature (15 °C), which highlights the presence of deeper groundwater circulation in the Western Andean Front. Boreholes groundwater temperature ranges from 18.6° (no. 30) to 23.2 °C (no. 7, 22). The pH values, ranging between 6.9 (no. 29) and 8.5 °C (no. 15), do not show a significant spatial variation.

The hydrogeochemical facies of groundwater along the Western Andean Front is mainly HCO_3-Ca (Fig. 3). That facies results from the dissolution of Ca-silicate minerals containing into the volcano-sedimentary rocks of the study area (see Sect. 4.2.2). In addition, we observed that two sample points (no. 12, 29) located at the downstream of PFZ are SO_4-Ca, which suggests a higher residence time of groundwater. The spring no. 3 is HCO_3-Na likely due to the dissolution of Na-silicate minerals into dykes observed in the field. The relation between EC and elevation is also visible in the variation of elements concentrations in groundwater (Fig. 4), where the concentrations are lowest in high-elevation areas and progressively increase down to the San Felipe aquifer. Note that samples located in the basin have a significant increase in the concentrations of Cl, NO_3, Sr and Ba instead of the samples located into the fractured rock (Fig. 4a, g, h and i).

4.2. Hydrogeochemical processes in the Western Andean Front

4.2.1. Groundwater evolution along flow paths

The hierarchical cluster analysis (HCA) reveals three main clusters (C1, C2 and C3; Fig. 5), whose average properties are summarized in the Table 5 and Fig. 5b. C1 includes all boreholes of the San Felipe aquifer (no. 6, 7, 21, 22, 23, 29, 30, 31) and springs with the highest electrical conductivity values (no. 12, 28). C2 includes the springs and boreholes located in the lowest and middle part of the Western Andean Front. C2 can be subdivided in two sub-groups (C2.1 and C2.2) composed of (i) springs outflowing from fractured rocks within the PFZ (no. 5, 14, 17, 18, 19, 20, 25, 26, 27) and boreholes into Quaternary colluvium deposits in PFZ (no. 16, 24); and (ii) springs outflowing in the middle part of the Western Andean Front from fractured rocks (no. 3, 4, 10, 11, 13, 15, 33). C3 includes the springs in highest elevations of the Western Andean Front (C3.1: no. 1, 2, 8, 9, 32) and meteoric waters (C3.2: no. 34, 35, 36, 37, 38). The Euclidian distance between C1 and C2 is lower than between C1-C2 and C3 (Fig. 5a). This reveals that C1 and C2 are geochemically more similar respect with C3. In addition, average properties inferred from HCA (Table 5) highlight that element concentrations (electrical conductivity) increase with decreasing elevation (Fig. 5b). However, the proportion of major elements is preserved from the upstream parts of the Western Andean Front up to the basin at the downstream. Those results seem to indicate that the variation of mineralization is due to an increase of the residence time rather than changes of geochemical reactions.

To test the previous assumption, we compared concentrations in both groundwater and meteoric water with data of leaching-rocks sampled in the study area. Considering the regional mineral proportions (Fuentes et al., 2004), dominated by Ca-plagioclase (anorthite) and in lower proportions by Na-plagioclase (albite) and CaMg-Pyroxenes, we examined the ionic ratios Na/Ca and Mg/Ca against the Cl (Fig. 6a and b). These reveal a well-defined gradual evolution of the groundwater concentrations from C3 up to C1 samples and tend to reach the composition of the host-rocks. Li and B are useful to characterize common sources of dissolved ions in waters (Nicholson, 1993). Li/Cl (Fig. 6c) and B/Cl (Fig. 6d) reveal that the source of dissolved ions in high elevation springs (C3) is due to meteoric water input, while most of groundwater in the Western Andean Front (C1 and C2) originates from the dissolution of the host-rocks. Hence, we state that the increase of groundwater mineralization is due to the residence time of groundwater that circulates in the Western Andean Front.

4.2.2. Source of dissolved ions: water-rock interactions and anthropogenic influences

Regarding previous findings, now we attempt to define the geochemical reactions and processes that occur along the Western Andean Front flow paths.

In the study area, the volcano-sedimentary rocks are compositionally andesitic (Table 2), whose the principal minerals are plagioclases. In the Andes of Central Chile there is the whole family of plagioclases,

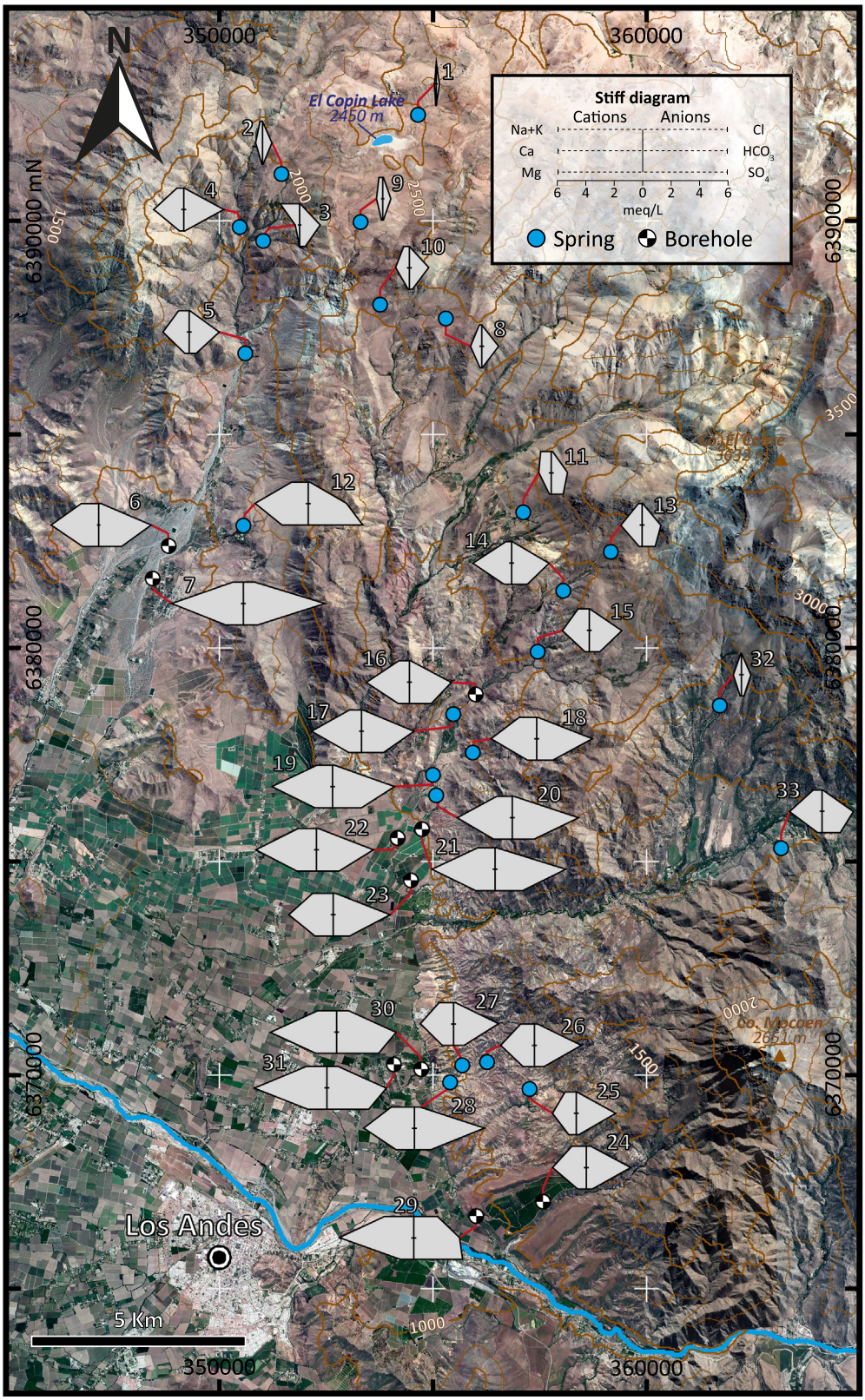

Fig. 3. Stiff diagrams of groundwater samples at the study area.

ranging from Na-plagioclase (albite) to Ca-plagioclase (anorthite), with labrodarite as an intermediate plagioclase (Fuentes et al., 2004). The dissolution of plagioclase occurs in presence of carbonic acid, derived from soil CO_2 dissolution (Eq. (1)). Albite (Na-plagioclase), labradorite (intermediate plagioclase) and anorthite (Ca-plagioclase) release a ratio of 1:1 of Na/HCO_3 (Eq. (2)), 1:3 of Na and Ca/HCO_3 (Eq. (3)), and 1:2 of Ca/HCO_3 (Eq. (4)), respectively (Fig. 7) (Elango and Kannan, 2007; Frengstad and Banks, 2007; Lerman and Wu, 2008).

$$H_2O + CO_2 \leftrightarrow H_2CO_3 \quad (1)$$

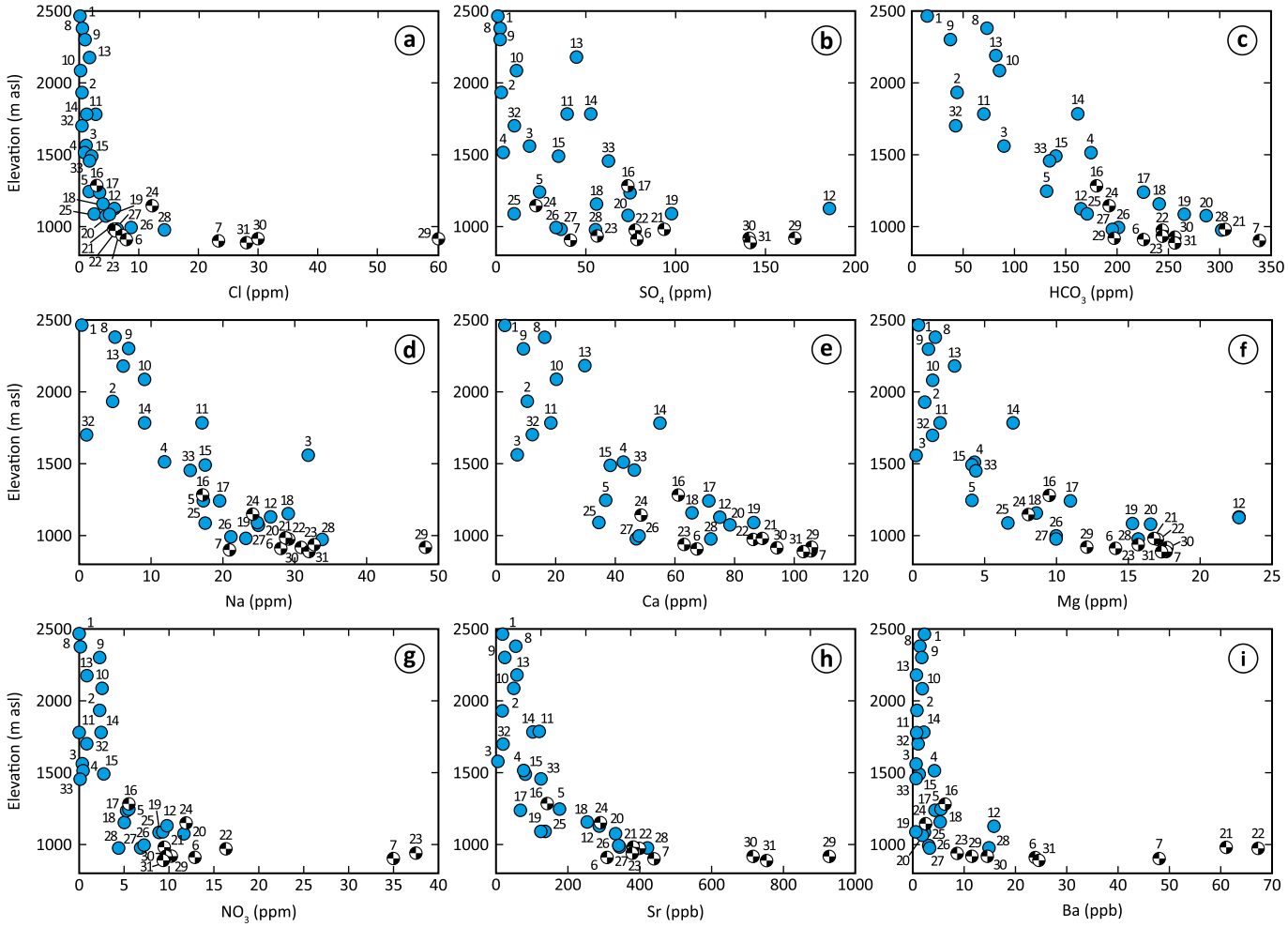

Fig. 4. Dissolved elements concentration *vs.* elevation (m asl) of springs (sky-blue) and boreholes (black and white) water samples.

$$\boldsymbol{NaAlSi_3O_8} + CO_2 + 2H_2O \leftrightarrow \boldsymbol{Na^+} + 3SiO_2 + Al(OH)_3 + \boldsymbol{HCO_3^-} \quad (2)$$

$$\boldsymbol{NaCaAl_3Si_5O_{16}} + 8CO_2 + 9H_2O \leftrightarrow \boldsymbol{2Na^+} + \boldsymbol{2Ca^2} + + 4SiO_2 + 3Al_2Si_2O_5(OH)_4 + \boldsymbol{6HCO_3^-} \quad (3)$$

$$\boldsymbol{CaAl_2Si_2O_8} + 2CO_2 + 4H_2O \leftrightarrow \boldsymbol{Ca^2} + + 2SiO_2 + Al(OH)_3 + \boldsymbol{2HCO_3^-} \quad (4)$$

We observe a positive correlation of Na and Ca with respect to HCO_3 (Fig. 7). Na *vs.* HCO_3 (Fig. 7a) shows that most samples fit to the 1:3-trend showing a main dissolution of labradorite. In turn, Ca *vs.* HCO_3 (Fig. 7b) shows that most samples plot between 1:3 and 1:2 stoichiometric lines, but tend to the 1:2-trend. These observations indicate the main role of anorthite dissolution in groundwater composition, even though labradorite dissolution occurs in a minor proportion. Our results agree with the proportion of plagioclase minerals in the study area, where anorthite is dominant (Fuentes et al., 2004). Thus, the plagioclase dissolution explained the amounts of Na, Ca and HCO_3.

In turn, the factorial analysis (FA) results in two factors (F1 and F2), which explain 82.6% of the total variance. These two factors suggest different sources of the analyzed variables (Fig. 8a). Factor 1 (58.25%) shows the statistical association of SO_4, HCO_3, Na, Ca, Mg, SiO_2, Li, B, As and Sr. Considering that the source of Na, Ca and HCO_3 is the dissolution of plagioclases (see above), we state that Factor 1 highlights the water-rock interaction processes. Factor 2 (24.37%) shows the statistical association of Cl, NO_3, Sr and Ba. Please note that agriculture activities in the study area release in soils: (i) fertilizers containing NO_3 and Sr (*e.g.* Fernández et al., 2016; Biddau et al., 2019; Kawagoshi et al., 2019); (ii) rodenticides with compounds of Ba (*personal observation during field work*); and iii) organochlorine pesticides (Cl) (*e.g.* Pozo et al., 2017; Cao et al., 2019; Climent et al., 2019). We assume that Factor 2 is related to anthropogenic influence (agriculture). However, the weight of Cl and NO_3 (Table 3) suggests that water-rock interaction may also contribute to the Cl and NO_3 concentrations in groundwater as supported by rock composition (Table 2).

In addition, the distribution of each sample with respect to the F1 and F2 (Fig. 8b) shows that C3 has negative scores in both factors. C3.2 (meteoric water) reveals that neither water-rock interaction (F1) nor anthropogenic activities (F2) influence the water composition. Despite that C3.1 shows negatives scores in F1, it reveals a minor influence of water-rock interactions processes in the groundwater of high-elevation springs. C2 shows positive values of F1 (up to ~1), which evidences the main role of water-rock interaction in the groundwater composition of the samples located at mid- and low-elevation in the Western Andean Front (C2.1 and C2.2). Finally, C1 has positive values in both factors, reflecting the gradual influence of the anthropogenic activities into groundwater composition (F1 reaches ~0.8, while F2 reaches ~2.0). Note that for samples with F2 values higher than F1 values, the anthropogenic activity is assumed predominant rather than the water-rock interaction, such as visible in the boreholes no. 6, 7, 21, 22, 29, 30, 31.

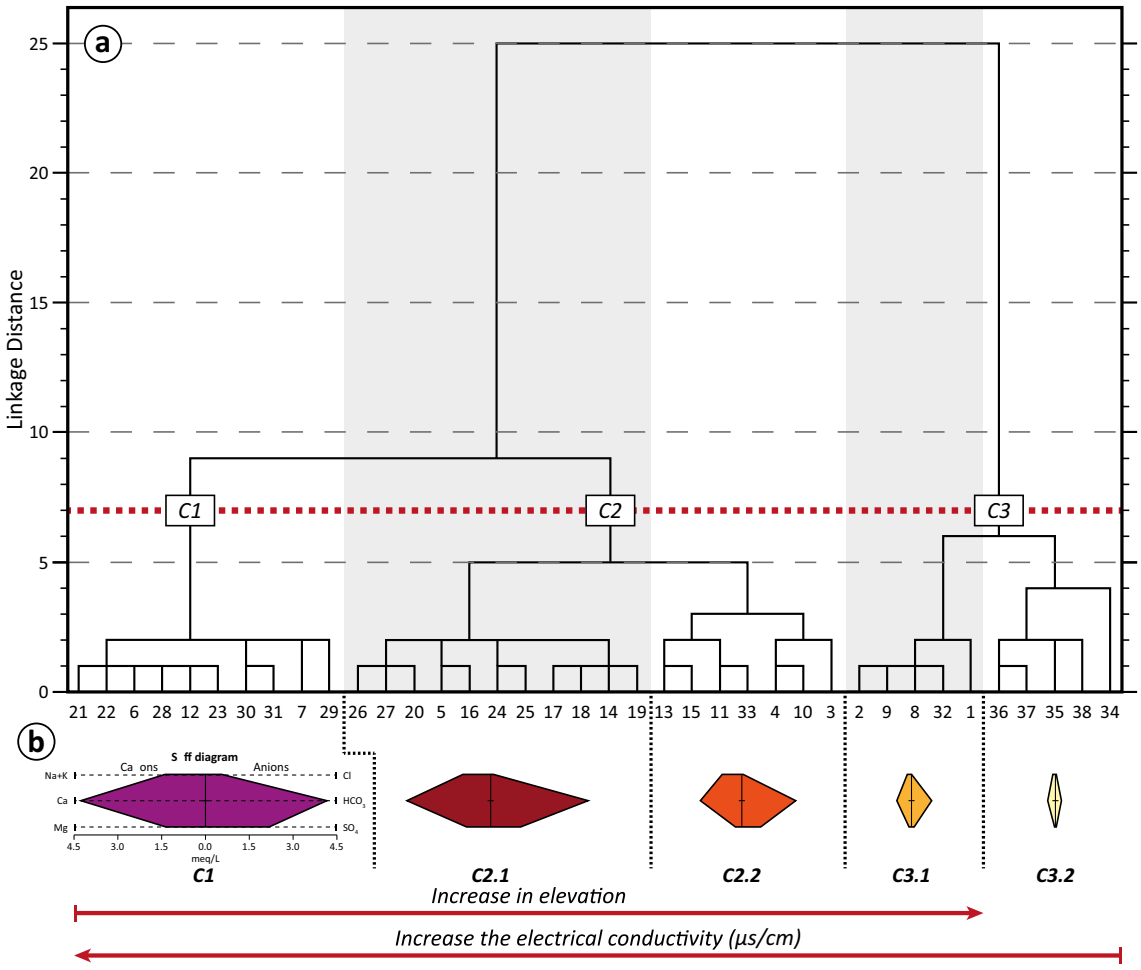

Fig. 5. Hierarchical cluster analysis. a) Dendogram shows the three main clusters. b) Stiff diagrams represent the average concentration of major ions in meq/l.

4.3. Water stable isotopes and groundwater origins

4.3.1. The 33°S Chile MWL

Inferred from regional annual precipitation weight means, the "*33°S Chile MWL*" is $\delta D = 8.07\delta^{18}O + 11.42$ ($R^2 = 0.97$) (Fig. 9a), and shows a similarity with the global meteoric water line GMWL ($\delta D = 8\delta^{18}O + 10$) (Craig, 1961). The regional influence of the orographic-continental effect is expressed by a gradient with elevation ($\nabla_z\delta^{18}O_P$) of −0.30‰ per 100 m asl (Fig. 9b) like one estimated by Sánchez-Murillo et al. (2018) for entire Chile (−0.347‰ per 100 m). For collected precipitation events (no. 35, 36, 37), $\delta^{18}O$ and δD analyses agree with "*33°S Chile MWL*" strengthening the representativeness for studying local hydrological processes. In addition, snowpack isotope compositions in the Principal Cordillera (Ohlanders et al., 2013) perfectly match with "*33°S Chile MWL*" (Fig. 9a) although a deviation is observed with the regional elevation gradient (Fig. 9b). This deviation results from abrupt topographic variations in the sub-catchments of the Principal Cordillera (narrow valleys with abrupt flanks). Snowpack isotope compositions correspond to elevations above 3000 m asl (Fig. 9b). Therefore, the provided "*33°S Chile MWL*" is robust for characterizing both the origin of groundwater and the related recharge processes in the study area, but also in other catchments of Central Chile.

4.3.2. Areas contributing to recharge groundwater

The contents of $\delta^{18}O$ and δD of springs range from −13.15‰ to −6.31‰ and from −92.56‰ to −69.52‰, respectively; and $\delta^{18}O$ and δD at boreholes range from −15.38‰ to −9.41‰ and − 107.92‰ to −78.30‰, respectively (Table 1). The comparison between groundwater and "*33°S Chile MWL*" shows that the groundwater originates from precipitation which took place over hydroclimatic conditions similar

Table 5
Average values of chemical composition for each water cluster identified by the HCA.

HCA clusters	Samples	Altitude (m asl)	Water type	EC (µS/cm)	T°C	Major elements (ppm)									Trace elements (ppb)				
						SiO_2	Cl	SO_4	HCO_3	NO_3	Na	K	Ca	Mg	Li	B	As	Sr	Ba
C1	6, 7, 12, 21, 22, 23, 28, 29, 30, 31	953	HCO_3-Ca	728	22	30.2	18.9	103.7	253.4	15.5	31.1	1.7	85.9	16.7	11.6	108.4	6.9	501.4	29.0
C2	5, 14, 16, 17, 18, 19, 20, 24, 25, 26, 27	1189	HCO_3-Ca	430	21	26.9	4.7	50.4	204.7	7.3	20.7	0.8	57.4	9.7	3.6	91.0	5.8	210.6	3.4
	3, 4, 10, 11, 13, 15, 33	1724	HCO_3-Ca	231	19	20.6	1.5	30.9	111.0	1.1	15.6	0.5	28.9	2.7	1.2	94.5	4.6	73.8	1.4
C3	1, 2, 8, 9, 32	2156	HCO_3-Ca	92	17	18.7	0.5	3.8	42.5	1.2	3.6	0.2	10.2	1.0	0.0	8.1	0.9	26.9	1.4
	34, 35, 36, 37, 38	–	HCO_3-Ca	39	15	0.4	1.0	2.1	12.6	0.4	0.5	2.8	5.1	0.3	0.1	9.7	1.0	10.9	5.1

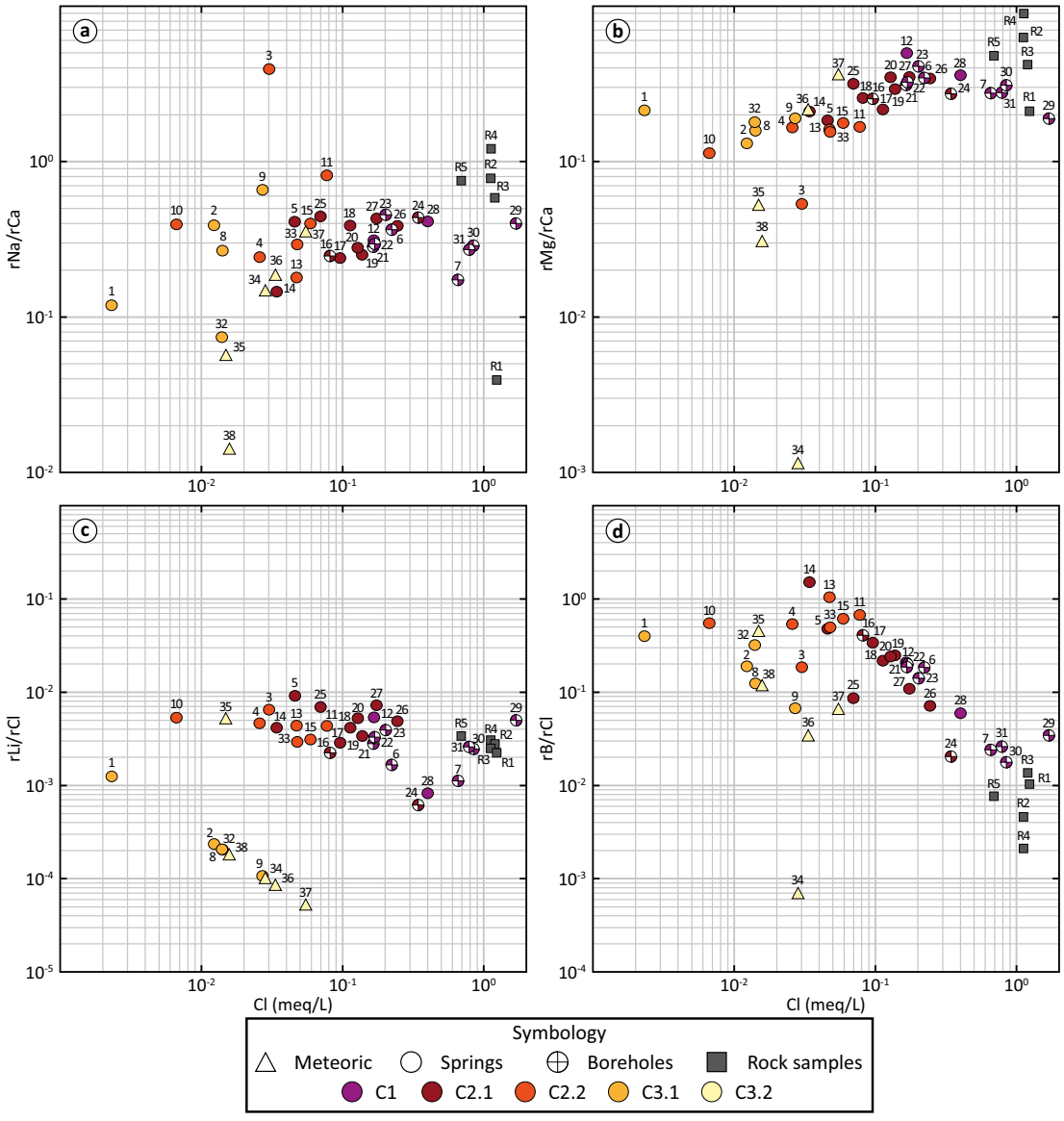

Fig. 6. Logarithmic ionic ratios calculated for water and rock samples *vs.* Cl (r = meq/L). The colour samples were classified according to HCA.

to the current ones (Fig. 9a). Most samples show an enrichment trend ($\delta D = 3.54\delta^{18}O$ - 45.42; $R^2 = 0.80$) indicating a partial evaporation of the meteoritic water. By the position of samples on this evaporation line, we noted an absence of negative relationship between partial evaporation rate (Fig. 9a) and the elevation of sampling points (Fig. 9b). This indicates that fractioning due to evaporation processes occurs locally during the surface-water infiltration rather than along the flow paths in the Western Andean Front. The slope of this enrichment trend (3.54) is typical of evaporation processes under dry conditions (Clark, 2015), which agrees with the semiarid conditions of the Aconcagua Basin.

At the interception between evaporation line and "*33°S Chile MWL*" (Fig. 9a), the value of $\delta^{18}O$ is −12.55‰. Regarding that, we estimate that the precipitation contributing to recharge groundwater takes place at around 2200 m asl (Fig. 9b). Involved recharge processes can be diffuse (direct process) in precipitation areas, but also focused (indirect process) into geomorphological structures (*e.g.* gullies) where runoff infiltrates. Nevertheless some springs (no. 1, 8, 9), related to precipitation at 2200 m asl (see above), are located between 2300 and 2500 m asl (Table 1). This altitude deviation is due to the wide range of meteoric isotope composition in high elevation sub-catchments and to the fractioning processes resulting of the evaporation and elution of snowpack (Ohlanders et al., 2013). Some samples (no. 21, 22, 23, 32, 33) could be also considered as not impacted by the evaporation (Fig. 9a). Regarding this uncertainty, we assume that precipitation at lower elevations (1800 and 2000 m asl; Fig. 9b) can also contribute to recharge the groundwater. Given that rain composition is similar to that of snow composition, we cannot distinguish if groundwater originates from residual rain (after evaporation) or snowmelt. Both origins are very likely.

The similarity of the vertical gradient (per 100 m a.s.l) of isotopic content in precipitation ($\nabla_z\delta^{18}O_P = -0.30‰$) and groundwater of springs ($\nabla_z\delta^{18}O_{GW\text{-}spring} = -0.29‰$) (Fig. 9b) indicates that groundwater of springs originates from local recharge processes rather than from a diffuse process along the slope of the mountain (Custodio and Jódar, 2016). In this latter case, the expected variation of the isotopic content in groundwater of springs with the elevation would be not linear, given that groundwater samples would be a mixture (groundwater regional discharge) of water originating from the upstream recharge areas and local infiltration (*i.e.* "slope effect"; Custodio and Jódar, 2016). Therefore, groundwater recharge occurs locally by focused indirect recharge processes through geomorphological structures such as fractures

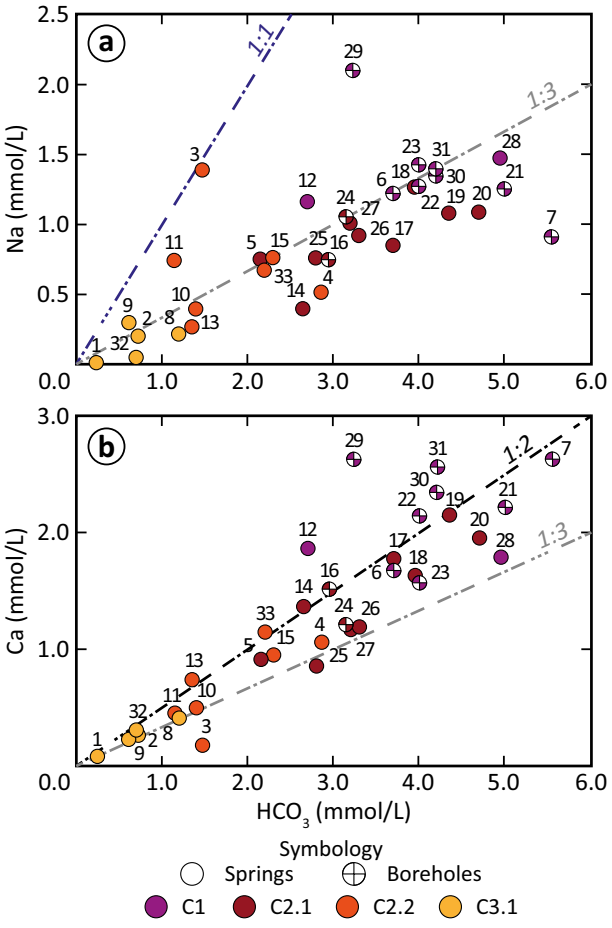

Fig. 7. Molar relationships of a) Na *vs.* HCO_3 and b) Ca *vs.* HCO_3 showing the plagioclase dissolution (stoichiometry ratios): albite (1:1), anorthite (1:2) and labradorite (1:3). The colour samples were classified according to HCA.

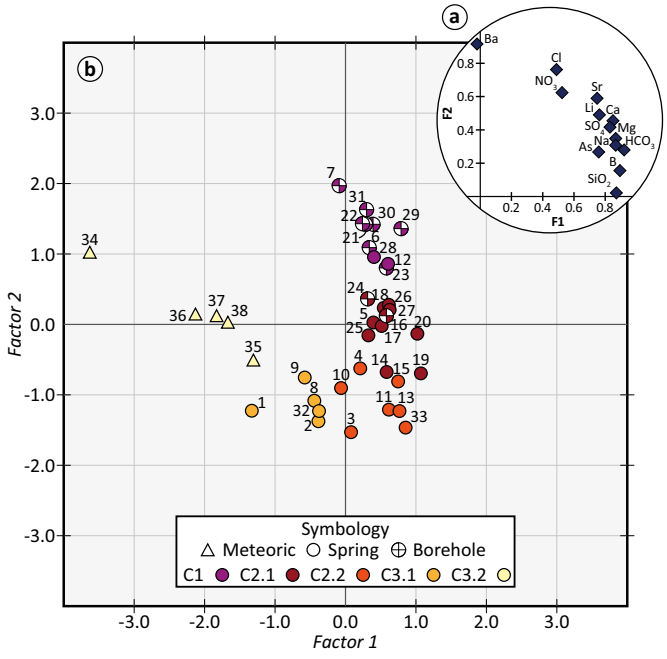

Fig. 8. Factorial analysis. a) Weight of the variables for Factor 1 and 2 (Table 3). b) Projection of factorial scores for the water samples. The colour samples were classified according to HCA.

and gullies. The isotopic content of springs groundwater can be also used to characterize the local precipitation altitudinal line for Central Chile. To the downstream of PFZ in Quaternary alluvial deposits (Fig. 1c), groundwater at the borehole no. 30 shows an isotopic inconsistency with respect to previous observation. The contents of $\delta^{18}O$ and δD are depleted and similar to the precipitation at ~3000 m asl (Fig. 9a and b) whereas the borehole no. 30 is located at 918 m asl. In addition, it does not show an enrichment process caused by the evaporation (Fig. 9a). In order to explain that, two assumptions must be cited: (i) A rapid and deep infiltration of rainy events at 3000 m asl through fractures without influence of evaporation. But to the East of this borehole (no. 30), the maximum elevation in the Western Andean Front is 2651 m asl (*Co. Mocoen*; Fig. 1c). This latter would imply a deep groundwater circulation originating from highs at about ten kilometres further East. But borehole no. 30 groundwater does not show a significant thermal property (18.8 °C; Table 1). (ii) A rapid transfer of surface water, from high-elevation areas in the Principal Cordillera (~3000 m asl) up to permeable alluvial deposits at downstream where surface water infiltrates. Indeed, a major irrigation canal is located at less than ~50 m of the borehole no. 30. This canal is devoid of impervious layer (field observation) and conducts water from the high parts of the Principal Cordillera up to the Central Depression (Fig. 1c).

Regarding previous information, canal-losses permit to recharge the groundwater of borehole no. 30 rather than supposed deep groundwater circulation coming from distant high-elevation areas. The $\delta^{18}O$ and δD analyses allow demonstrating the role of anthropogenic activities (irrigation canals) in the recharge of San Felipe aquifer.

4.4. Conceptual model and groundwater resources in the Western Andean Front

In the high-elevation sub-catchments (>2200 m asl), the rapid infiltration of snowmelt and rainstorms in fractures is relevant regarding the storage of groundwater in high-elevation areas (Fig. 10a and b). There, groundwater composition is poorly influenced by water-rock interactions. During dry years, the release of groundwater stored in high-elevation areas supports the shallow groundwater circulation (Ohlanders et al., 2013; Staudinger et al., 2017; Foks et al., 2018; Jódar et al., 2017; Glas et al., 2019), which feeds high-elevation springs and wetlands (López-Angulo et al., 2020). It is also a primary source of the groundwater recharge for Western Andean Front hydrogeological systems. The occurrence of such process is relevant considering the current and future hydroclimatic conditions of Central Chile (*i.e.* "Megadrought"; Garreaud et al., 2017, 2019). Nevertheless, climate predictions show a decrease in precipitation together with a decline of the snow cover area (Garreaud et al., 2017; Stehr and Aguayo, 2017). As a result, the contribution of high-elevation areas to the Western Andean Front groundwater recharge is today declining.

At lower elevations, below 2200 m asl (Fig. 10a), runoff and subsurface circulation coming from higher-elevation areas are concentrated in mid-mountain gullies and infiltrate at depth in fractures and colluvial deposits (Fig. 10b). Focused (indirect) recharge feeds springs located in the Western Andean Front. Local observers report a rapid and short increment of the spring discharge, located at the downstream in the PFZ (Fig. 10c), after rainy events and fast melting periods of the snow cover. Although our study does not address hydrodynamic changes, this information has to be considered. It indicates that groundwater circulation in fractured rocks is governed by piston flows. In the Western Andean Front the contents of HCO_3, Na, Ca, Mg and SiO_2 are governed by the dissolution of CaNa-plagioclase (labradorite), Ca-plagioclase (anorthite) and CaMg-pyroxenes. Other dissolved ions, such as SO_4, Li, B, As and Sr, originate from water-rock interactions despite that involved mineral reactions were not identified. We demonstrated that electrical conductivity results from previous reactions. The absence of different sources of dissolved ions as well as evapoconcentration processes along the flow paths in the Western

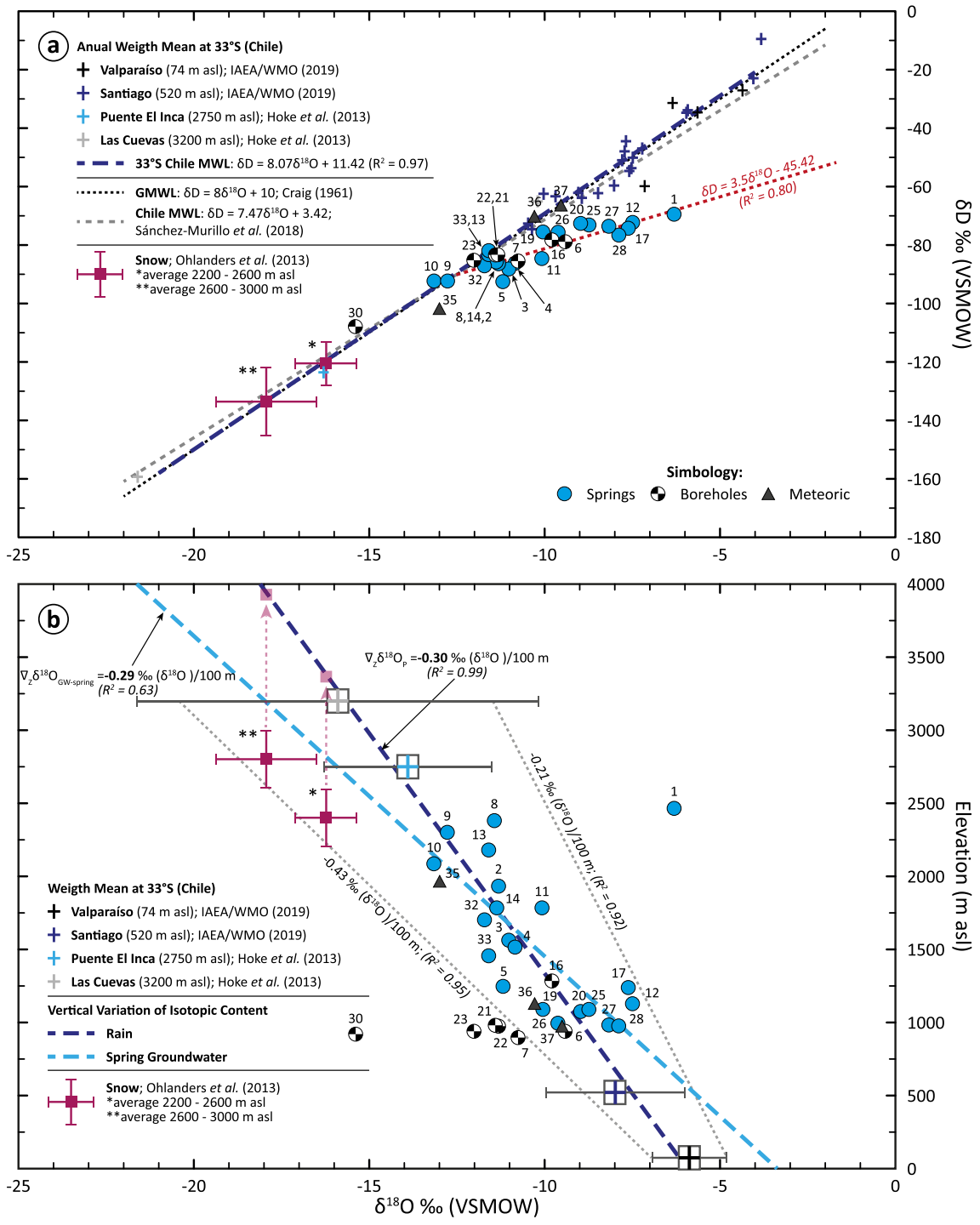

Fig. 9. Water stable isotopes. a) Relationship between δD *vs.* $\delta^{18}O$ and *33°S Chile MWL*. b) Orographic-continental effect on $\delta^{18}O$ values at 33°S. The vertical content of the isotopic content in groundwater ($\nabla_z\delta^{18}O_{GW\text{-}spring}$) along the Western Andean Front was calculated considering only the springs (no. 1 has not been included because it is very heavy related to the corresponding elevation).

Andean Front lead us to assume that the increment of the mineralization toward the downstream is due to an increase of the residence time. The analyses of NO_3 and As in groundwater (Fig. 11), hazardous elements for human health, reveal that the Western Andean Front groundwater is of relatively good quality, without anthropogenic pollution. All samples show NO_3 concentrations below the Chilean (NCh409/1) and international (WHO) drinking water limits (Fig. 11a). Regarding As concentrations (Fig. 11b), some samples (no. 12, 13, 20) exceed the established limits for drinking water. However those points are not used for drinking water purposes, but they can be used for mineral bottling water (Daniele et al., 2019). Indeed, these samples are below the Chilean Decree 106 (Fig. 11b).

In the downstream part of the Western Andean Front (Fig. 10a and e), the occurrence of low-thermal groundwater circulation (up to 9 °C above the local mean annual air temperature) indicates that deep flows contribute to recharge the San Felipe Aquifer. The mountain-block recharge process (Wilson and Guan, 2004) is related to groundwater flows coming from recharge areas in the Western Andean Front (see above) and circulating by interconnected fractures (PFZ) up to the downstream adjacent alluvial basin (focused recharge). Oblique

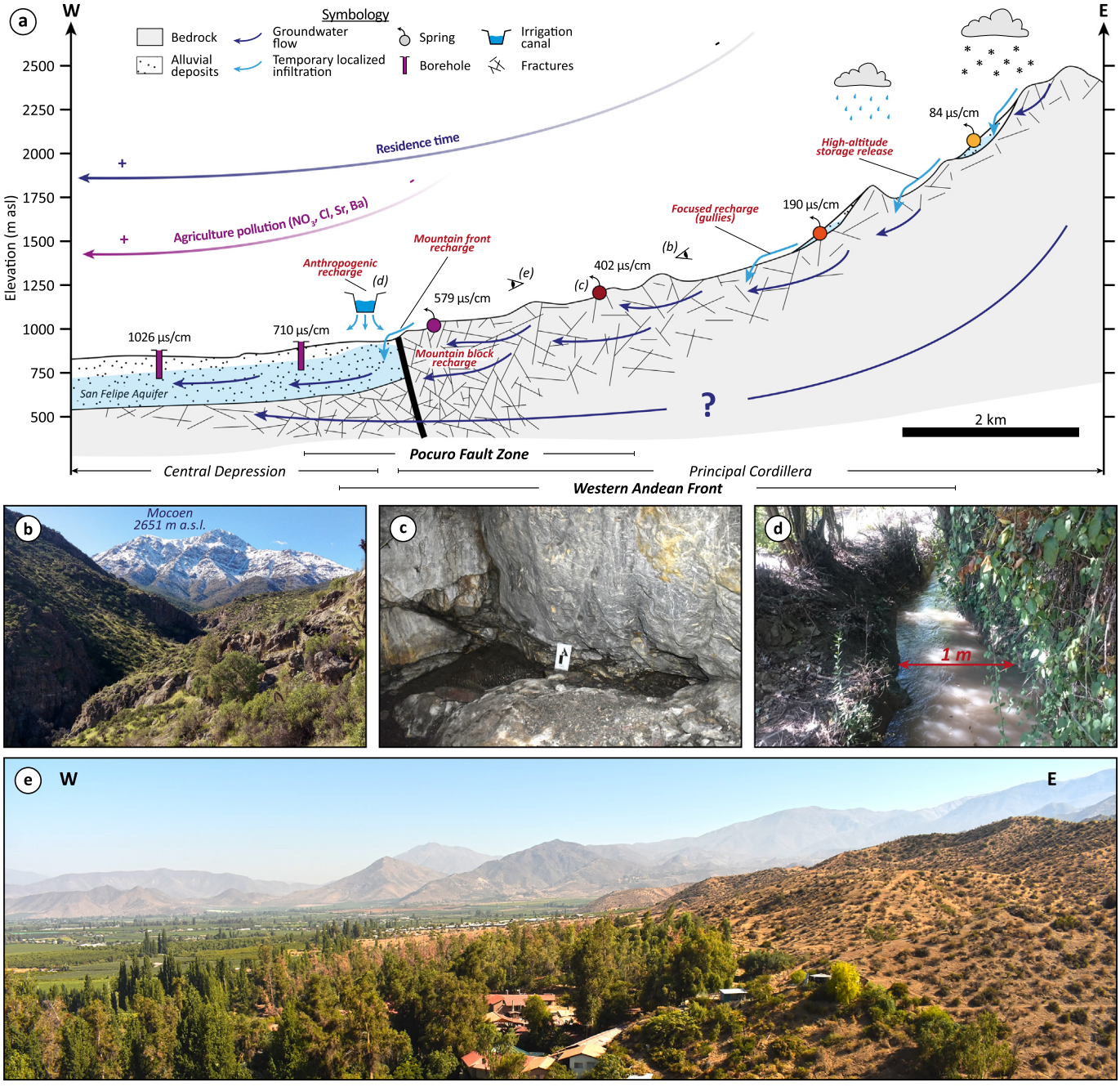

Fig. 10. Hydrogeological conceptual model of the Western Andean Front. Colours of the springs are related to the HCA clusters.

basements faults crossing the mountain front zone are typically considered as high-permeability axes allowing a focused recharge of adjacent alluvial aquifers (Wilson and Guan, 2004; Kebede et al., 2008; Taillefer et al., 2018; Walter et al., 2019). Despite an absence of direct evidences, a topological relation has been observed between oblique basement faults and major groundwater circulation in Central Chile (Oyarzún et al., 2017; Piquer et al., 2019). Such process would permit a permanent recharge of the San Felipe Aquifer, between 5 and 50% of the total alluvial aquifer recharge (Markovich et al., 2019). In addition, at the downstream of the mountain front zone shaped by PFZ (Fig. 10e), the focused and rapid infiltration of streams in coarse alluvial deposits also contributes to recharge the San Felipe Aquifer (Fig. 10a). This process originates from the perennial infiltration of secondary rivers (Fig. 1c) fed by high-elevation springs as well as the infiltration of ephemeral streams triggered by rainstorms on dry soils of the Western Andean Front. In addition to previous natural processes, there is another process related to agriculture activities (Fig. 10a and d). Water originating from high elevation areas is rapidly transferred down to irrigation canals localized in the Central Depression (Fig. 1c). The absence of impervious layer at canal bottoms (Fig. 10d) promotes a permanent and focused infiltration (Barberá et al., 2018) and therefore an artificial groundwater recharge, historically used in the Andes (Ochoa-Tocachi et al., 2019). Subsequently, the groundwater in the alluvial aquifer has an isotopic composition similar to high-elevation precipitation (Fig. 9). In Central Depression, the infiltration from agriculture practices (fertilizers) impacted the groundwater quality by an increase of NO_3 concentration. Moreover, the increase of Cl, Sr, and Ba concentrations in groundwater is statically related to the agriculture (organochlorine pesticides, fertilizers and rodenticides inputs). Given that groundwater coming from the Western Andean Front has a good quality, we note that a change

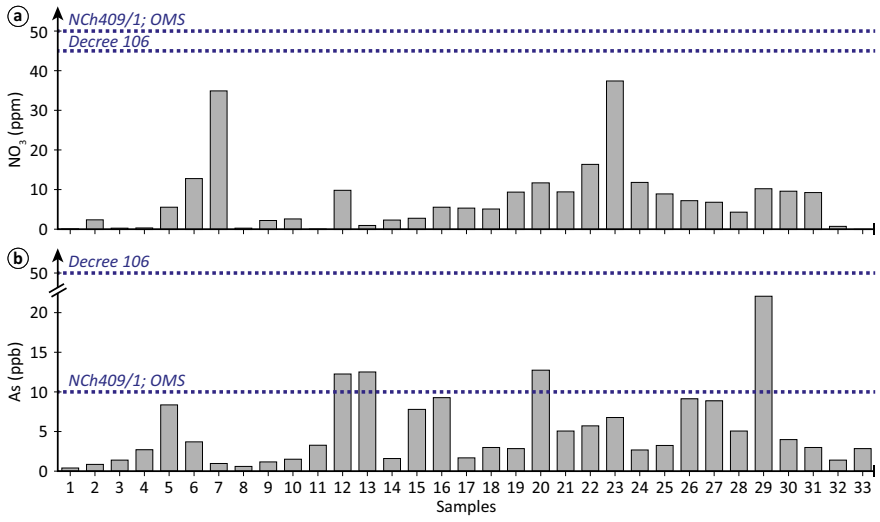

Fig. 11. Drinking water quality limits according with national (NCh409/1) and international (WHO) drinking water limits, and mineral bottling water (Decree no. 106) for a) NO_3 and b) As.

of agriculture practices will help for diminishing the presence of human-origin hazardous components in the San Felipe Aquifer. About a quantitative aspect, current dry years have promoted the implementation of impermeable infrastructures for diminishing water losses from canal-infiltration. Our findings reveal that the implementation of an impervious layer at canal bottoms will dramatically impact the renewal of the San Felipe Aquifer.

5. Conclusion

This research addresses the groundwater resources and related recharge processes in the Western Andean Front (Central Chile) at the Aconcagua Basin by hydrogeochemical, rock compositions and water isotopes analyses. Unlike former considerations, we demonstrate the existence of groundwater circulation in fractured rocks originating from rain and snowmelt above ~2000 m asl. Groundwater recharge occurs in gullies at mid-elevation and feeds springs located at the downstream. Mountain-block and mountain-front recharge processes contribute to recharge the Central Depression alluvial aquifers. In addition, we demonstrate that irrigation canals (conducting water from high-elevation areas) play a significant role in the recharge of Central Depression aquifers impacting the groundwater isotope composition. Groundwater in the Western Andean Front has a high-quality according to the national (NCh409/1 and Decree 106) and international (WHO) limits of element concentrations for different water-uses (drinking water, mineral bottling water, thermal baths and irrigation). However, intensive agriculture practices in the Central Depression lead to a decline of the groundwater quality in alluvial aquifers by an increase of hazardous elements for human-health.

So far, studies have considered the Western Andean Front as a no-flux boundary condition in flow modelling. But our findings highlight that the Western Andean Front must be considered for estimating the renewal of the Central depression alluvial aquifers. It is also an interesting target for the exploration of groundwater resources, especially regarding the current alarming state of water resources in Central Chile. Therefore, we invite to use this original conceptual model to improve the established groundwater resource management policies in Central Chile, due to the similar hydroclimatic and geological contexts of the Aconcagua Basin.

Acknowledgements

Financial support was exclusively provided by *Agencia Nacional de Investigación y Desarrollo de Chile* (ANID) through the public funding programs: FONDECYT no. 1170569, FONDAP no. 15090013 (Andean Geothermal Center of Excellence, CEGA), FONDEQUIP EQM120098, ECOS-CONICYT no. 180055/C18U03 and ITAL170012. The PhD studies of Matías Taucare are funded by ANID-*Beca Doctorado Nacional* no. 21160325. The authors acknowledge to Verónica Rodríguez, Samuel Lepe and Erika Rojas who performed the water chemical analysis and the leaching-rock test at CEGA labs. We also thank to PhD Antonio Delgado of *Instituto Andaluz de Ciencias de la Tierra* (CSIC-*Universidad de Granada*) who performed the analysis of stable isotopes. We sincerely appreciate the collaboration of *Termas El Corazón*, *Termas de Jahuel*, *Fundo El Barro, APR Santa Filomena*, *Sky El Arpa*, *Agrícola El Triunfo* and Segundo Pereira for facilitating our field works. Finally, special thanks to Marcelo Cortés, Carlo Divasto, Angello Negri, Léa Théodose and Vanessa Treskow for their field support. Thanks to Omara Fernández for the English revision.

References

Arancibia, G., 2004. Mid-cretaceous crustal shortening: evidence from a regional-scale ductile shear zone in the Coastal Range of central Chile (32° S). J. S. Am. Earth Sci. 17 (3), 209–226. https://doi.org/10.1016/j.jsames.2004.06.001.

Aravena, R., Suziki, O., Peña, H., Pollastri, A., Fuenzalida, H., Grilli, A., 1999. Isotopic composition and origin of the precipitation in Northern Chile. Appl. Geochem. 14 (4), 411–422. https://doi.org/10.1016/S0883-2927(98)00067-5.

Armijo R., Rauld R., Thiele R., Vargas G., Campos J., Lacassin R. & Kausel E. 2010. The West Andean Thrust, the San Ramón Fault, and the seismic hazard for Santiago, Chile. Tectonics 29 (2), TC2007. doi:https://doi.org/10.1029/2008TC002427.

Barberá, J.A., Jódar, J., Custodio, E., González-Ramón, A., Jiménez-Gavilán, P., Vadillo, I., Pedrera, A., Martos-Rosillo, S., 2018. Groundwater dynamics in a hydrologically-modified alpine watershed from an ancient managed recharge system (Sierra Nevada National Park, southern Spain): insights from hydrogeochemical and isotopic information. Sci. Total Environ. 640–641, 874–893. https://doi.org/10.1016/j.scitotenv.2018.05.305.

Barrett, B.S., Garreaud, R.D., Falvey, M., 2009. Effect of the Andes Cordillera on precipitation from a midlatitude cold front. Mon. Weather Rev. 137, 3092–3109. https://doi.org/10.1175/2009MWR2881.1.

Benavente, O., Tassi, F., Reich, M., Aguilera, F., Capecchiacci, F., Gutiérrez, F., Vaselli, O., Rizzo, A., 2016. Chemical and isotopic features of cold and thermal fluids discharged in the Southern Volcanic Zone between 32.5°S and 36°S: insights into the physical and chemical processes controlling fluid geochemistry in geothermal systems of Central Chile. Chem. Geol. 420, 97–113. https://doi.org/10.1016/J.CHEMGEO.2015.11.010.

Biddau, R., Cidu, R., Da Pelo, S., Carletti, A., Ghiglieri, G., Pittalis, D., 2019. Source and fate of nitrate in contaminated groundwater systems: assessing spatial and temporal variations by hydrogeochemistry and multiple stable isotope tools. Sci. Total Environ. 647, 1121–1136. https://doi.org/10.1016/j.scitotenv.2018.08.007.

Boisier, J.P., Rondanelli, R., Garreaud, R.D., Muñoz, F., 2016. Anthropogenic and natural contributions to the Southeast Pacific precipitation decline and recent megadrought in central Chile. Geophys. Res. Lett. 43 (1), 413–421. https://doi.org/10.1002/2015GL067265.

Boyce D., Charrier R. & Farias M. 2020. The first Andean compressive tectonic phase. Sedimentologic and structural analysis of mid-Cretaceous deposits in the Coastal

Cordillera, Central Chile (32°50'S). Tectonics 39 (2), e2019TC005825. doi:10.1029/2019TC005825.
Bustamante, M., Lemus, M., Cortés, R., Vivallos, J., Cáceres, D., Wall, R., 2012. Exploración geológica para el fomento de la energía geotérmica: Área de Jahuel, Región de Valparaíso. Servicio Nacional de Geología y Minería (SERNAGEOMIN). Chile, Santiago.
Cao, F., Jaunat, J., Sturchio, N., Cancès, B., Morvan, X., Devos, A., Barbin, V., Ollivier, P., 2019. Worldwide occurrence and origin of perchlorate ion in waters: a review. Sci. Total Environ. 661, 737–749. https://doi.org/10.1016/j.scitotenv.2019.01.107.
Charrier, R., Baeza, O., Elgueta, S., Flynn, J.J., Gans, P., Ka, S.M., Muñoz, N., Wyss, A.R., Zurita, E., 2002. Evidence for Cenozoic extensional basin development and tectonic inversion south of the flat-slab segment, southern Central Andes, Chile (33°-36°S.L.). J. S. Am. Earth Sci. 15 (1), 117–139. https://doi.org/10.1016/S0895-9811(02)00009-3.
Charrier, R., Pinto, L., Rodríguez, M.P., 2007. In: Moreno, T., Gibbons, W. (Eds.), Tectonostratigraphic Evolution of the Andean Orogen in Chile. Geological Society of London, pp. 21–114. https://doi.org/10.1144/GOCH.3 The Geology of Chile.
Clark, I., 2015. Groundwater Geochemistry and Isotopes. 1st ed. CRC Press https://doi.org/10.1201/b18347 456 pp.
Climent, M.J., Coscollà, C., López, A., Barra, R., Urrutia, R., 2019. Legacy and current-use pesticides (CUPs) in the atmosphere of a rural area in central Chile, using passive air samplers. Sci. Total Environ. 662, 646–654. https://doi.org/10.1016/j.scitotenv.2019.01.302.
Cloutier, V., Lefebvre, R., Therrien, R., Savard, M.M., 2008. Multivariate statistical analysis of geochemical data as indicative of the hydrogeochemical evolution of groundwater in a sedimentary rock aquifer system. J. Hydrol. 353 (3–4), 294–313. https://doi.org/10.1016/j.jhydrol.2008.02.015.
Cortés, G., Vargas, X., McPhee, J., 2011. Climatic sensitivity of streamflow timing in the extratropical western Andes Cordillera. J. Hydrol. 405 (1–2), 93–109. https://doi.org/10.1016/j.jhydrol.2011.05.013.
Costumero, R., Sánchez, J., García-Pedrero, A., Rivera, D., Lillo, M., Gonzalo-Martín, C., Menasalvas, E., 2016. Geography of legal water disputes in Chile. Journal of Maps 13 (1), 7–13. https://doi.org/10.1080/17445647.2016.1252803.
Craig, H., 1961. Isotopic variations in meteoric waters. Science 133 (3465), 1702–1703. https://doi.org/10.1126/science.133.3465.1702.
Custodio, E., Jódar, J., 2016. Simple solutions for steady–state diffuse recharge evaluation in sloping homogeneous unconfined aquifers by means of atmospheric tracers. J. Hydrol. 540, 287–305. https://doi.org/10.1016/j.jhydrol.2016.06.035.
Daniele, L., Cannatelli, C., Buscher, J.T., Bonatici, G., 2019. Chemical composition of Chilean bottled waters: anomalous values and possible effects on human health. Sci. Total Environ. 689, 526–533. https://doi.org/10.1016/j.scitotenv.2019.06.165.
Darapsky, L., 1890. Las aguas minerales en Chile. Imprenta del Universo de Guillermo Helfmann. 196.
Darwin C. 1839. The Voyage of the Beagle. Wordsworth, vol. 733 p.
DGA, 2015. Determinación de la Disponibilidad de Aguas Subterráneas en el Valle del Río Aconcagua. Dirección General de Aguas (DGA), Santiago, Chile.
DGA. 2016. Disponibilidad de Recursos Hídricos para el Otorgamiento de Derechos de Aprovechamiento de Aguas Subterráneas en el Valle del Aconcagua: Sectores hidrogeológicos de San Felipe, Putaendo, Panquehue, Catemu y Llay Llay. Dirección General de Aguas (DGA), Santiago, Chile.
DGA. 2019. Inventario Público de Información Hidrológica y Meteorológica. Dirección General de Aguas (DGA), Santiago, Chile. http://snia.dga.cl/BNAConsultas/reportes.
DPRH, 2015. Política Nacional para los Recursos Hídricos. Santiago, Chile.
Elango, L., Kannan, R., 2007. Rock–water interaction and its control on chemical composition of groundwater. In: Sarkar, D., Datta, R., Hannigan, R. (Eds.), Concepts and Applications in Environmental Geochemistry. 5. Elsevier, pp. 229–243. https://doi.org/10.1016/S1474-8177(07)05011-5.
Farías M., Comte D., Charrier R., Martinod J., David C., Tassara A., Tapia F. & Fock A. 2010. Crustal-scale structural architecture in central Chile based on seismicity and surface geology: implications for Andean mountain building. Tectonics 29 (3), TC3006. doi: 10.1029/2009TC002480.
Fernández, E., Grilli, A., Alvarez, D., Aravena, R., 2016. Evaluation of nitrate levels in groundwater under agricultural fields in two pilot areas in central Chile: a hydrogeological and geochemical approach. Hydrol. Process. 31 (6), 1206–1224. https://doi.org/10.1002/hyp.11103.
Filzmoser, P., Hron, K., Reimann, C., 2009. Univariate statistical analysis of environmental (compositional) data: problems and possibilities. Sci. Total Environ. 407 (23), 6100–6108. https://doi.org/10.1016/J.SCITOTENV.2009.08.008.
Foks, S.S., Stets, E.G., Singha, K., Clow, D.W., 2018. Influence of climate on alpine stream chemistry and water sources. Hydrol. Process. 32 (13), 1993–2008. https://doi.org/10.1002/hyp.13124.
Frengstad, B., Banks, D., 2007. Universal controls on the evolution of groundwater chemistry in shallow crystalline rock aquifers: The evidence from empirical and theoretical studies. In: Krásný, J., Sharp, J.M. (Eds.), Groundwater in Fractured Rocks: IAH Selected Paper Series. CRC Press, pp. 275–289.
Fuentes, F., 2004. Petrología y metamorfismo de muy bajo grado de unidades volcánicas oligoceno-miocenas en la ladera occidental de Los Andes de Chile Central (33°S). (PhD Thesis). Universidad de Chile. Santiago, Chile.
Fuentes, F., Vergara, M., Aguirre, L., Féraud, G., 2002. Contact relationships of Tertiary volcanic units from the Andes of Central Chile (33°S): a reinterpretation based on $^{40}Ar/^{39}Ar$ dating. Revista Geológica de Chile 29 (2), 151–165.
Fuentes, F., Aguirre, L., Vergara, M., Valdebenito, L., Fonseca, E., 2004. Miocene fossil hydrothermal system associated with a volcanic complex in the Andes of Central Chile. J. Volcanol. Geotherm. Res. 138 (1–2), 139–161. https://doi.org/10.1016/j.jvolgeores.2004.07.001.
Gamboa, C., Godfrey, L., Herrera, C., Custodio, E., Soler, A., 2019. The origin of solutes in groundwater in a hyper-arid environment: a chemical and multi-isotope approach in the Atacama Desert, Chile. Sci. Total Environ. 690, 329–351. https://doi.org/10.1016/j.scitotenv.2019.06.356.
Gana, P., Wall, R., 1997. Evidencias geocronológicas 40Ar/39Ar y K-Ar de un hiatus cretácico superior-eoceno en Chile central (33-33° 30'S). Revista Geológica de Chile 24 (2), 145–163.
Garreaud, R.D., 2009. The Andes climate and weather. Adv. Geosci. 22, 3–11. https://doi.org/10.5194/adgeo-22-3-2009.
Garreaud, R.D., 2013. Warm winter storms in Central Chile. J. Hydrometeorol. 14, 1515–1534. https://doi.org/10.1175/JHM-D-12-0135.1.
Garreaud, R.D., Lopez, P., Minvielle, M., Rojas, M., 2013. Large-scale control on the Patagonian climate. J. Clim. 26, 215–230. https://doi.org/10.1175/JCLI-D-12-00001.1.
Garreaud, R.D., Alvarez-Garreton, C., Barichivich, J., Boisier, J.P., Christie, D., Galleguillos, M., LeQuesne, C., McPhee, J., Zambrano-Bigiarini, M., 2017. The 2010–2015 megadrought in central Chile: impacts on regional hydroclimate and vegetation. Hydrol. Earth Syst. Sci. 21 (12), 6307–6327. https://doi.org/10.5194/hess-21-6307-2017.
Garreaud, R.D., Boisier, J.P., Rondanelli, R., Montecinos, A., Sepúlveda, H.H., Veloso-Aguila, D., 2019. The Central Chile mega drought (2010–2018): a climate dynamics perspective. Int. J. Climatol., 1–19 https://doi.org/10.1002/joc.6219.
Giménez-Forcada, E., Vega-Alegre, M., Timón-Sánchez, S., 2017. Characterization of regional cold-hydrothermal inflows enriched in arsenic and associated trace-elements in the southern part of the Duero Basin (Spain), by multivariate statistical analysis. Sci. Total Environ. 593–594, 211–226. https://doi.org/10.1016/j.scitotenv.2017.03.071.
Glas, R., Lautz, L., McKenzie, J., Moucha, R., Chavez, D., Mark, B., Lane Jr., J.W., 2019. Hydrogeology of an alpine talus aquifer: Cordillera Blanca, Peru. Hydrogeol. J. 27 (6), 2137–2154. https://doi.org/10.1007/s10040-019-01982-5.
Godoy, E., Yañez, G., Vera, E., 1999. Inversion of an Oligocene volcano-tectonic basin and uplifting of its superimposed Miocene magmatic arc in the Chilean Central Andes: first seismic and gravity evidences. Tectonophysics 306 (2), 217–236. https://doi.org/10.1016/S0040-1951(99)00046-3.
Güler, C., Thyne, G.D., McCray, J.E., Turner, A.K., 2002. Evaluation of graphical and multivariate statistical methods for classification of water chemistry data. Hydrogeol. J. 10 (4), 455–474. https://doi.org/10.1007/s10040-002-0196-6.
Güngör, H., Elik, A., 2007. Comparison of ultrasound-assisted leaching with conventional and acid bomb digestion for determination of metals in sediment samples. Microchem. J. 86 (1), 65–70. https://doi.org/10.1016/J.MICROC.2006.10.006.
Hauser, A., 1997. Catastro y caracterización de las fuentes de aguas minerales y termales de Chile. Servicio Nacional de Geología y Minería (SERNAGEOMIN). Chile, Santiago.
Hoke, G.D., Aranibar, J.N., Viale, M., Araneo, D.C., Llano, C., 2013. Seasonal moisture sources and the isotopic composition of precipitation, rivers, and carbonates across the Andes at 32.5-35.5°S. Geochem. Geophys. Geosyst. 14 (4), 962–978. https://doi.org/10.1002/ggge.20045.
Houston, J., 2002. Groundwater recharge through an alluvial fan in the Atacama Desert, northern Chile: mechanisms, magnitudes and causes. Hydrol. Process. 16 (15), 3019–3035. https://doi.org/10.1002/hyp.1086.
Huggenberger, P., Aigner, T., 1999. Introduction to the special issue on aquifer-sedimentology: problems, perspectives and modern approaches. Sediment. Geol. 129 (3–4), 179–186. https://doi.org/10.1016/S0037-0738(99)00101-3.
IAEA/GNIP, 2014. Precipitation sampling guide.
IAEA/WMO, 2019. Global network of isotopes in precipitation. The GNIP Database http://nucleus.iaea.org/wiser.
Janke, J.R., Ng, S., Bellisario, A., 2017. An inventory and estimate of water stored in firn fields, glaciers, debris-covered glaciers, and rock glaciers in the Aconcagua River Basin, Chile. Geomorphology 296, 142–152. https://doi.org/10.1016/j.geomorph.2017.09.002.
Jara, P., Charrier, R., 2014. New stratigraphical and geochronological constraints for the Mezo-Cenozoic deposits in the High Andes of central Chile between 32° and 32°30'S: structural and palaeogeographic implications. Andean Geol. 41 (1), 174–209. https://doi.org/10.5027/andgeoV41n1-a07.
Jódar, J., Cabrera, J.A., Martos-Rosillo, S., Ruiz-Constán, A., González-Ramón, A., Lambán, L.J., Herrera, C., Custodio, E., 2017. Groundwater discharge in high-mountain watersheds: a valuable resource for downstream semi-arid zones. The case of the Bérchules River in Sierra Nevada (southern Spain). Sci. Total Environ. 593–594, 760–772. https://doi.org/10.1016/j.scitotenv.2017.03.190.
Jordan, T.E., Isacks, B., Allmendinger, R., Brewer, J., Ramos, V., Aando, C., 1983. Andean tectonics related to geometry of subducted Nazca plate. GSA Bull. 94 (3), 341–361. https://doi.org/10.1130/0016-7606(1983)94<341:ATRTGO>2.0.CO;2.
Jordan, T.E., Burns, W.M., Veiga, R., Pángaro, F., Copeland, P., Kelley, S., Mpodozis, C., 2001. Extension and basin formation in the southern Andes caused by increased convergence rate: a mid-Cenozoic trigger for the Andes. Tectonics 20 (3), 308–324. https://doi.org/10.1029/1999TC001181.
Jorquera, C.O., Oates, C.J., Plant, J.A., Kyser, K., Ihlenfeld, C., Voulvoulis, N., 2015. Regional hydrogeochemical mapping in Central Chile: natural and anthropogenic sources of elements and compounds. Geochemistry: Exploration, Environment, Analysis 15 (1), 72–96. https://doi.org/10.1144/geochem2013-220.
Kaasalainen, H., Stefánsson, A., 2012. The chemistry of trace elements in surface geothermal waters and steam, Iceland. Chem. Geol. 330–331, 60–85. https://doi.org/10.1016/j.chemgeo.2012.08.019.
Kawagoshi, Y., Suenaga, Y., Chi, N., Hama, T., Ito, H., Duc, L., 2019. Understanding nitrate contamination based on the relationship between changes in groundwater levels and changes in water quality with precipitation fluctuations. Sci. Total Environ. 657, 146–153. https://doi.org/10.1016/j.scitotenv.2018.12.041.
Kay, S.M., Godoy, E., Kurtz, A., 2005. Episodic arc migration, crustal thickening, subduction erosion, and magmatism in the south-central Andes. Bull. Geol. Soc. Am. 117 (1–2), 67–88. https://doi.org/10.1130/B25431.1.

Kayser, H.F., 1960. The application of electronic computers to factor analysis. Educational and Physochological Measurement 20 (1), 141–151. https://doi.org/10.1177/001316446002000116.
Kebede, S., Travi, Y., Asrat, A., Alemayehu, T., Ayenew, T., Tessema, Z., 2008. Groundwater water origin and flow along selected transects in Ethiopian rift volcanic aquifers. Hydrogeol. J. 16 (1), 55–73. https://doi.org/10.1007/s10040-007-0210-0.
Kresic, N., Mikszewski, A., 2012. Hydrogeological Conceptual Site Models: Data Analysis and Visualization. 1st ed. CRC Press https://doi.org/10.1201/b12151 600 pp.
Lerman, A., Wu, L., 2008. Kinetics of global geochemical cycles. In: Brantley, S., Kubicki, J., White, A. (Eds.), Kinetics of Water-Rock Interaction. Springer, pp. 655–736. https://doi.org/10.1007/978-0-387-73563-4_13.
López-Angulo, J., Pescador, D.S., Sánchez, A.M., Luzuriaga, A.L., Cavieres, L.A., Escudero, A., 2020. Impacts of climate, soil and biotic interactions on the interplay of the different facets of alpine plant diversity. Sci. Total Environ. 698, 133960. https://doi.org/10.1016/j.scitotenv.2019.133960.
Magaritz, M., Aravena, R., Peña, H., Suzuki, O., Grilli, A., 1990. Source of ground water in the deserts of northern Chile: evidence of deep circulation of ground water from the Andes. Groundwater 28 (4), 513–517. https://doi.org/10.1111/j.1745-6584.1990.tb01706.x.
Marazuela, M.A., Vázquez-Suñé, E., Ayora, C., García-Gil, A., Palma, T., 2019. Hydrodynamics of salt flat basins: the Salar de Atacama example. Sci. Total Environ. 651, 668–683. https://doi.org/10.1016/j.scitotenv.2018.09.190 Part 1.
Markovich, K.H., Manning, A.H., Condon, L.E., McIntosh, J.C., 2019. Mountain-block recharge: a review of current understanding. Water Resour. Res. 55. https://doi.org/10.1029/2019WR025676.
Matusiewicz, H., 2003. Wet digestion methods. In: Mester, Z.M., Sturgeon, R. (Eds.), Sample Preparation for Trace Element Analysis. 41. Elsevier, pp. 193–233. https://doi.org/10.1016/S0166-526X(03)41006-4.
Moeck, C., Radny, D., Borer, P., Rothardt, J., Auckenthaler, A., Berg, M., Schirmer, M., 2016. Multicomponent statistical analysis to identify flow and transport processes in a highly-complex environment. J. Hydrol. 542, 437–449. https://doi.org/10.1016/j.jhydrol.2016.09.023.
Montecinos, A., Aceituno, P., 2003. Seasonality of the ENSO-related rainfall variability in central Chile and associated circulation anomalies. J. Clim. 16, 281–296. https://doi.org/10.1175/1520-0442(2003)016<0281:SOTERR>2.0.CO;2.
Moya, C.E., Raiber, M., Taulis, M., Cox, M.E., 2015. Hydrochemical evolution and groundwater flow processes in the Galilee and Eromanga basins, Great Artesian Basin, Australia: a multivariate statistical approach. Sci. Total Environ. 508, 411–426. https://doi.org/10.1016/J.SCITOTENV.2014.11.099.
Mpodozis C. & Ramos V. 1989. The Andes of Chile and Argentina. In: Ericksen G.E., Cañas-Pinochet M.T. & Reinemund J. (Eds.), Geology of the Andes and its relation to hydrocarbon and mineral resources. Circum-Pacific Counsil for Energy and Mineral Resources, 59–90.
Muñoz, M., Fuentes, F., Vergara, M., Aguirre, L., Nyström, J., Féraud, G., Demant, A., 2006. Abanico East Formation: petrology and geochemistry of volcanic rocks behind the Cenozoic arc front in the Andean Cordillera, central Chile (33°50'S). Revista Geológica de Chile 33 (1), 109–140. https://doi.org/10.5027/andgeoV33n1-a05.
Negri, A., Daniele, L., Aravena, D., Muñoz, M., Delgado, A., Morata, D., 2018. Decoding fjord water contribution and geochemical processes in the Aysen thermal springs (southern Patagonia, Chile). J. Geochem. Explor. 185, 1–13. https://doi.org/10.1016/J.GEXPLO.2017.10.026.
Nester, P.L., Gayó, E., Latorre, C., Jordan, T.E., Blanco, N., 2007. Perennial stream discharge in the hyperarid Atacama Desert of northern Chile during the latest Pleistocene. Proceedings of the National Academy of Sciences of the USA 104 (50), 19724–19729. https://doi.org/10.1073/pnas.0705373104.
Nicholson, K., 1993. Geothermal Fluids: Chemistry and Exploration Techniques. Springer, p. 263. https://doi.org/10.1007/978-3-642-77844-5.
NOAA/National Weather Service, 2019. El Niño Southern Oscilation (ENSO): Historical El Niño/La Niña Episodes (1950-Present). https://origin.cpc.ncep.noaa.gov/products/analysis_monitoring/ensostuff/ONI_v5.php.
Novoa, V., Ahumada-Rudolph, R., Rojas, O., Sáez, K., de la Barrera, F., Arumí, J.L., 2019. Understanding agricultural water footprint variability to improve water management in Chile. Sci. Total Environ. 670, 188–199. https://doi.org/10.1016/j.scitotenv.2019.03.127.
Nyström, J., Vergara, M., Morata, D., Levi, B., 2003. Tertiary volcanism during extension in the Andean foothills of central Chile (33°15′–33°45′S). Geol. Soc. Am. Bull. 115 (12), 1523–15237. https://doi.org/10.1130/B25099.1.
Ochoa-Tocachi, B.F., Bardales, J.D., Antiporta, J., Pérez, K., Acosta, L., Mao, F., Zulkafli, Z., Gil-Ríos, J., Angulo, O., Grainger, S., Gammie, G., De Bièvre, B., buytaert, W., 2019. Potential contributions of pre-Inca infiltration infrastructure to Andean water security. Nature Sustainability 2, 584–593. https://doi.org/10.1038/s41893-019-0307-1.
Ohlanders, N., Rodriguez, M., McPhee, J., 2013. Stable water isotope variation in a central Andean watershed dominated by glacier and snowmelt. Hydrol. Earth Syst. Sci. 17, 1035–1050. https://doi.org/10.5194/hess-17-1035-2013.
Oyarzún, R., Oyarzún, J., Fairley, J.P., Núñez, J., Gómez, N., Arumí, J.L., Maturana, H., 2017. A simple approach for the analysis of the structural-geologic control of groundwater in an arid rural, mid-mountain, granitic and volcanic-sedimentary terrain: the case of the Coquimbo Region, North-Central Chile. J. Arid Environ. 142, 31–35. https://doi.org/10.1016/J.JARIDENV.2017.03.003.
Parada, M.A., Rivano, S., Sepulveda, P., Herve, M., Herve, F., Puig, A., Munizaga, F., Brook, M., Pankhurst, R., Snelling, N., 1988. Mesozoic and cenozoic plutonic development in the Andes of central Chile (30°30′-32°30'S). J. S. Am. Earth Sci. 1 (3), 249–260. https://doi.org/10.1016/0895-9811(88)90003-X.
Piquer, J., Hollings, P., Rivera, O., Cooke, D.R., Baker, M., Testa, F., 2017. Along-strike segmentation of the Abanico Basin, central Chile: new chronological, geochemical and structural constraints. Lithos 268–271, 174–197. https://doi.org/10.1016/j.lithos.2016.10.025.
Piquer, J., Yañez, G., Rivera, O., Cooke, D.R., 2019. Long-lived crustal damage zones associated with fault intersections in the high Andes of Central Chile. Andean Geol. 46, 223–239. https://doi.org/10.5027/andgeoV46n2-3106.
Pozo, K., Oyola, G., Estellano, V.H., Harner, T., Rudolph, A., Prybilova, P., Kukucka, P., Audi, O., Klánová, J., Metzdorff, A., Focardi, S., 2017. Persistent Organic Pollutants (POPs) in the atmosphere of three Chilean cities using passive air samplers. Sci. Total Environ. 586, 107–114. https://doi.org/10.1016/j.scitotenv.2016.11.054.
Rauld, R., 2011. Deformación cortical y peligro sísmico asociado a la falla San Ramón en el frente cordillerano de Santiago, Chile Central (33°S) (PhD Thesis). Universidad de Chile. Santiago, Chile.
Rivano, S., Godoy, E., Vergara, M., Villarroel, R., 1990. Redefinición de la formación farellones en la Cordillera de los Andes de Chile central (32-34°5). Revista Geológica de Chile 17 (2), 205–214.
Rivano, S., Sepúlveda, P., Boric, R., Espiñeira, D., 1993. Hojas Quillota y Portillo, Escala 1: 250. Servicio Nacional de Geología y Minería (SERNAGEOMIN), Santiago, Chile, p. 000.
Rivera, D., Godoy-Faúndez, A., Lillo, M., Alvez, A., Delgado, V., Gonzalo-Martín, C., Menasalvas, E., Costumero, R., García-Pedrero, A., 2016. Legal disputes as a proxy for regional conflicts over water rights in Chile. J. Hydrol. 535, 36–45. https://doi.org/10.1016/j.jhydrol.2016.01.057.
Sánchez-Murillo, R., Aguirre-Dueñas, E., Gallardo-Amestica, M., Moya-Vega, P., Birkel, C., Esquivel-Hernández, G., Boll, J., 2018. Isotopic characterization of waters across chile. In: Rivera, D.A., Godoy-Faundez, A., Lillo-Saavedra, M. (Eds.), Andean Hydrology. CRC Press, pp. 205–230. https://doi.org/10.1201/9781315155982-9.
Scanlon, B.R., Keese, K.E., Flint, A.L., Flint, L.E., Gaye, C.B., Edmunds, W.M., Simmers, I., 2006. Global synthesis of groundwater recharge in semiarid and arid regions. Hydrol. Process. 20 (15), 3335–3370. https://doi.org/10.1002/hyp.6335.
Schaffer, N., MacDonell, S., Réveillet, S., Réveillet, M., Yáñez, E., Valois, R., 2019. Rock glaciers as a water resource in a changing climate in the semiarid Chilean Andes. Reg. Environ. Chang. 19 (5), 1263–1279. https://doi.org/10.1007/s10113-018-01459-3.
Simmers, I., 1997. In: Simmers, I. (Ed.), Groundwater Recharge Principles, Problems and Developments. CRC Press, pp. 1–18 Recharge of phreatic aquifers in (semi-)arid areas.
Staudinger, M., Stoelzle, M., Seeger, S., Seibert, J., Weiler, M., Stahl, K., 2017. Catchment water storage variation with elevation. Hydrol. Process. 31 (11), 2000–2015. https://doi.org/10.1002/hyp.11158.
Stehr, A., Aguayo, M., 2017. Snow cover dynamics in Andean watersheds of Chile (32.0–39.5° S) during the years 2000–2016. Hydrol. Earth Syst. Sci. 21 (10), 5111–5126. https://doi.org/10.5194/hess-21-5111-2017.
Taillefer, A., Guillou-Frottier, L., Soliva, R., Magri, F., Lopez, S., Courrioux, G., Millot, R., Ladouche, B., Le Goff, E., 2018. Topographic and faults control of hydrothermal circulation along dormant faults in an Orogen. Geochemistry. Geophysics, Geosystems 19 (12), 4972–4995. https://doi.org/10.1029/2018GC007965.
Thomas H. 1958. Geología de la cordillera de la costa entre el Valle de La Ligua y la Cuesta de Barriga. Servicio Nacional de Geología y Minería (SERNAGEOMIN), Santiago, Chile.
Valdés-Pineda, R., Pizarro, R., García-Chevesich, P., Valdés, J.B., Olivares, C., Vera, M., Balocchi, F., Pérez, F., Vallejos, C., Fuentes, R., Abarza, A., Helwig, B., 2014. Water governance in Chile: availability, management and climate change. J. Hydrol. 519, 2538–2567. https://doi.org/10.1016/j.jhydrol.2014.04.016 Part C.
Vargas, G., Klinger, Y., Rockwell, T.K., Forman, S.L., Rebolledo, S., Baize, S., Lacassin, R., Armijo, R., 2014. Probing large intraplate earthquakes at the west flank of the Andes. Geology 42 (12), 1083–1086. https://doi.org/10.1130/G35741.1.
Viale, M., Garreaud, R.D., 2014. Summer precipitation events over the Western slope of the subtropical Andes. Mon. Weather Rev. 142, 1074–1092. https://doi.org/10.1175/MWR-D-13-00259.1.
Viguier, B., Jourde, H., Yáñez, G., Lira, E.S., Leonardi, V., Moya, C.E., García-Pérez, T., Maringue, J., Lictevout, E., 2018. Multidisciplinary study for the assessment of the geometry, boundaries and preferential recharge zones of an overexploited aquifer in the Atacama Desert (Pampa del Tamarugal, northern Chile). J. S. Am. Earth Sci. 86, 366–383. https://doi.org/10.1016/J.JSAMES.2018.05.018.
Viguier, B., Daniele, L., Jourde, H., Leonardi, V., Yañez, G., 2019. Changes in the conceptual model of the Pampa del Tamarugal aquifer: implications for central depression water resources. J. S. Am. Earth Sci. 94, 102217. https://doi.org/10.1016/j.jsames.2019.102217.
Wall, R., Sellés, D., Gana, P., 1999. Área Tiltil-Santiago, región Metropolitana, Escala 1:100. Servicio Nacional de Geología y Minería (SERNAGEOMIN), Santiago, Chile, p. 000.
Walter, B., Géraud, Y., Hautevelle, Y., Diraison, M., Raisson, F., 2019. Fluid circulations at structural intersections through the Toro-Bunyoro fault system (Albertine Rift, Uganda): a multidisciplinary study of a composite hydrogeological system. Geofluids 20. https://doi.org/10.1155/2019/8161469.
Wang, P., Sun, Z., Hu, Y., Cheng, H., 2019. Leaching of heavy metals from abandoned mine tailings brought by precipitation and the associated environmental impact. Sci. Total Environ. 695, 133893. https://doi.org/10.1016/j.scitotenv.2019.133893.
Waylen, P.R., Caviedes, C.N., 1990. Annual and seasonal fluctuations of precipitation and streamflow in the Aconcagua River basin, Chile. J. Hydrol. 120 (1–4), 79–102. https://doi.org/10.1016/0022-1694(90)90143-L.
Wilson, J.L., Guan, H., 2004. Mountain-block hydrology and mountain-front recharge. In: Hogan, J.F., Phillips, F.M., Scanlon, B.R. (Eds.), Groundwater Recharge in a Desert Environment: The Southwestern United States. 9, pp. 113–137 American Geophysical Union.
Yáñez, G., Muñoz, M., Flores-Aqueveque, V., Bosch, A., 2015. Gravity depth to basement in Santiago Basin, Chile: implications for its geological evolution, hydrogeology, low enthalpy geothermal, soil characterization and geo-hazards. Andean Geol. 42 (2), 147–172. https://doi.org/10.5027/andgeoV42n2-a01.